© 2022. Published by The Company of Biologists Ltd | Journal of Cell Science (2022) 135, jcs259811. doi:10.1242/jcs.259811

RESEARCH ARTICLE

N-acetylation of secreted proteins in Apicomplexa is widespread and is independent of the ER acetyl-CoA transporter AT1

Mary Akinyi Nyonda[1], Jean-Baptiste Boyer[2], Lucid Belmudes[3], Aarti Krishnan[1], Paco Pino[1,4], Yohann Couté[3], Mathieu Brochet[1], Thierry Meinnel[2,*], Dominique Soldati-Favre[1,*] and Carmela Giglione[2,*]

ABSTRACT

Acetyl-CoA participates in post-translational modification of proteins and in central carbon and lipid metabolism in several cell compartments. In mammals, acetyl-CoA transporter 1 (AT1, also known as SLC33A1) facilitates the flux of cytosolic acetyl-CoA into the endoplasmic reticulum (ER), enabling the acetylation of proteins of the secretory pathway, in concert with the activity of dedicated acetyltransferases such as NAT8. However, the involvement of the ER acetyl-CoA pool in acetylation of ER-transiting proteins in Apicomplexa is unknown. Here, we identified homologs of AT1 and NAT8 in *Toxoplasma gondii* and *Plasmodium berghei* parasites. Proteome-wide analyses revealed widespread N-terminal acetylation of secreted proteins in both species. Such extensive acetylation of N-terminally processed proteins has not been observed previously in any other organism. Deletion of *AT1* homologs in both *T. gondii* and *P. berghei* resulted in considerable reductions in parasite fitness. In *P. berghei*, AT1 was found to be important for growth of asexual blood stages, production of female gametocytes and male gametocytogenesis, implying its requirement for parasite transmission. In the absence of AT1, lysine acetylation and N-terminal acetylation in *T. gondii* remained globally unaltered, suggesting an uncoupling between the role of AT1 in development and active acetylation occurring along the secretory pathway.

KEY WORDS: *Toxoplasma gondii*, *Plasmodium berghei*, Acetyl-CoA transporter, Acetylation, Secretory pathway, Endoplasmic reticulum

INTRODUCTION

Plasmodium spp. and *Toxoplasma gondii*, which are members of the phylum Apicomplexa, are obligate intracellular parasites of clinical relevance, causing malaria and toxoplasmosis, respectively. In the search for newer, safer and more efficient drugs or vaccines to combat these diseases there is an urgent need for the identification of novel cellular targets for intervention, particularly given the continuous emergence of resistance to available drugs.

Acetyl-CoA is a membrane-impermeable metabolite made up of an acetyl (CH_3CO) group joined to coenzyme A. It plays a central role in protein modification, as well as in lipid and central carbon metabolism, and is a promising target for antimalarials (de Vries et al., 2021). In both *T. gondii* and *Plasmodium* spp., acetyl-CoA is produced in the mitochondria in an atypical manner through activity of the branched-chain α-keto acid dehydrogenase (BCKDH) complex, which uses pyruvate as a substrate. In the apicoplast, a relict plastid organelle derived from secondary endosymbiosis, pyruvate is converted to acetyl-CoA by the pyruvate dehydrogenase (PDH) complex (Fleige et al., 2007; Cobbold et al., 2013). In the nucleo-cytosol compartment of *T. gondii*, two routes of production are implemented: through acetyl-CoA synthetase (ACS), using acetate as a substrate, and through ATP citrate lyase (ACL, also known as ATP citrate synthase), which uses citrate (Tymoshenko et al., 2015). In contrast, cytosolic acetyl-CoA is only produced through ACS in *Plasmodium falciparum* (Cobbold et al., 2013). In-depth analysis of the contribution of these distinct acetyl-CoA pools to parasite physiology has revealed that abrogation of cytosolic production of acetyl-CoA in *T. gondii* leads to inhibition of fatty acid elongation, reduced lysine acetylation of 115 proteins in both secretory and nucleo-cytosolic compartments, and ultimately parasite death (Kloehn et al., 2020). Indeed, acetyl-CoA is also used by N-terminal α-acetyltransferases (NATs) and lysine acetyltransferases (KATs) to specifically modify by acetylation the N-termini or the side chains of lysines of proteins, respectively (Friedmann and Marmorstein, 2013; Montgomery et al., 2015; Drazic et al., 2016). Different NATs have been characterized based on their substrate specificity: NatA is a complex involved in N-terminal acetylation (NTA) of proteins in which the first methionine has been cleaved; NatB, NatC and NatE complexes modify proteins with N-terminal methionines; and NatD (also known as NAA40) and NatH (also known as NAA80) are specific for NTA of histone and actin isoforms, respectively (Aksnes et al., 2019).

Acetylation on both N-termini and side chains of lysine residues of proteins have been reported in both *T. gondii* and *Plasmodium* spp., and more than 1000 acetylated proteins have been identified in *P. falciparum* (Cobbold et al., 2016). Exported parasite proteins, including proteins that are directed to the surface of red blood cells (RBCs), have their signal peptides and host-targeting motifs cleaved by an endopeptidase, plasmepsin V, in the endoplasmic reticulum (ER) (Boddey et al., 2010; Russo et al., 2010; Osborne et al., 2010). An acetyl moiety is then transferred from acetyl-CoA to the newly formed N-termini by a specific but uncharacterized ER-resident acetyl-CoA acetyltransferase, priming the proteins for trafficking (Chang et al., 2008; Osborne et al., 2010). In *T. gondii* tachyzoites, trafficking of the majority of rhoptry and microneme proteins to their respective secretory organelles occurs through the ER and Golgi. Rhoptry discharge requires proteolytic maturation of proteins at the N-termini by aspartyl protease (ASP3), which is

[1]Department of Microbiology and Molecular Medicine, University of Geneva, Geneva 1211, Switzerland. [2]Université Paris-Saclay, CEA, CNRS, Institute for Intergrative Biology of the Cell (I2BC), 91198 Gif-sur-Yvette, France. [3]Université Grenoble Alpes, INSERM, CEA, UMR BioSanté U1292, CNRS, CEA, FR2048, 38000 Grenoble, France. [4]ExcellGene SA, CH1870 Monthey, Switzerland.

*Authors for correspondence (carmela.giglione@i2bc.paris-saclay.fr; dominique.soldati-favre@unige.ch; thierry.meinnel@i2bc.paris-saclay.fr)

M.A.N., 0000-0002-5271-5089; J.-B.B., 0000-0001-5265-3917; L.B., 0000-0002-3515-0055; A.K., 0000-0002-7936-4442; P.P., 0000-0001-9705-1389; Y.C., 0000-0003-3896-6196; M.B., 0000-0003-3911-5537; T.M., 0000-0001-5642-8637; D.S., 0000-0003-4156-2109; C.G., 0000-0002-7475-1558

Handling Editor: Michael Way
Received 26 January 2022; Accepted 5 May 2022

present at a post-Golgi location termed the endosome-like compartment (ELC) (Dogga et al., 2017). Furthermore, a subset of *T. gondii* GRA proteins undergo proteolytic cleavage by ASP5 at the Golgi (Hammoudi et al., 2015; Coffey et al., 2018).

In mammalian cells, acetyl-CoA is actively translocated into the ER lumen via acetyl-CoA transporter 1 (AT1, also known as SLC33A1), a polytopic membrane protein belonging to a family of symporters localized in the ER membrane (Jonas et al., 2010). AT1-mediated import of acetyl-CoA into the ER facilitates acetylation of lysine residues on proteins by resident NAT8 acetyltransferases (Jonas et al., 2010; Pehar and Puglielli, 2013; Dieterich et al., 2019; Farrugia and Puglielli, 2018). Homologs of AT1 can be found in model organisms including *Saccharomyces cerevisiae*, *Caenorhabditis elegans* and *Drosophila melanogaster* (Hirabayashi et al., 2004) but not in the plastid-containing *Arabidopsis thaliana* plant model. Putative AT1 homologs have also been found to localize to the ER in *P. falciparum* (Lim et al., 2016) and *T. gondii* (Tymoshenko et al., 2015; Barylyuk et al., 2020). However, the importance of acetyl-CoA import into the ER and its role in post-translational acetylation of secreted proteins have not been investigated to date. Genome-wide fitness screens have revealed that *Plasmodium berghei AT1* (Pb*AT1*) contributes to the development of blood-stage forms (Bushell et al., 2017) and is essential for transmission to mosquitoes (Stanway et al., 2019). In contrast, *T. gondii AT1* (Tg*AT1*) has a fitness score of −0.07 according to the results of a CRISPR-Cas9 screen, suggesting that it might be dispensable during the tachyzoite stage in tissue culture (Sidik et al., 2016).

In this study, we performed an N-terminomics analysis of *T. gondii* and *P. berghei*. This analysis revealed the existence of a dedicated N-terminal protein processing machinery that mediates proteolysis followed by acetylation in several compartments within apicomplexan parasites, including the secretory pathway. Such frequent NTA of proteins of the secretory pathway has not been identified previously in any other organism. Taken together, the data presented here indicate the existence in these parasites of N-acyltransferases (NATs) that exhibit substrate specificity comparable to that observed for previously characterized NATs (NatA–E and NatH). Accordingly, homologs of several cytosolic NAT catalytic subunits could be identified in the proteomes of *T. gondii* and *P. berghei*. Among these, a NAT8 homolog is, so far, the only likely candidate NAT for ER-located protein acetylation, and it is essential for parasite growth. Likewise, AT1 is the only candidate to fuel the ER acetylation pathway, independently of the acetyltransferase activity involved. The gene encoding AT1 was deleted in *P. berghei* and *T. gondii*, resulting in considerable reduction in parasite fitness. Unexpectedly, global acetylome profiling of both N-α-termini and N-ε-lysine residues (acetylation of N-ε-lysine is hereafter referred to as K-acetylation) in both *T. gondii* and *P. berghei* AT1 knockout parasites revealed modest or no alteration of the acetylomes of secretory proteins. Overall, this study highlights the role of AT1 in parasite fitness and specifically in gametogenesis in *P. berghei*. This role is, however, not correlated with the protein acetylation of ER-transiting proteins, suggesting that a bypass alternative route ensures acetyl-CoA import along the secretory pathway in the absence of AT1.

RESULTS

N-terminomics analysis reveals the existence of a typical N-terminal protein processing machinery in Apicomplexa

The role of acetylation in the secretion pathway of apicomplexan parasites is poorly understood. We searched for evidence of acetyl-CoA occurrence through assessing protein acetylation marks on acceptor amino groups (i.e. N-α and N-ε groups) as these modifications rely on acetyl-CoA as an unique acetyl donor. In addition, widespread K-acetylation of proteins has been observed in various compartments of *T. gondii* RH strain parasites, including the ER (Kloehn et al., 2020; Jeffers and Sullivan, 2012; Xue et al., 2013). In contrast, only a few studies have reported on the maturation of proteins at the N-terminus and the machinery involved in apicomplexan parasites (Dogga et al., 2017; Chang et al., 2008). NTA profiles allow not only relative but also absolute quantitative measurements, with stoichiometric assessment of the acetylation yield (i.e. the amount of acetylated protein as a percentage of total acetylated and non-acetylated protein). To further investigate the protein acetylome of these parasites, we performed a global quantitative analysis of NTA in both *P. berghei* and *T. gondii* using the SILProNAQ procedure, which has been described previously (Frottin et al., 2016; Bienvenut et al., 2015). The SILProNAQ method facilitates identification of protein N-termini and quantification of NTA. The complete unfiltered data search yielded 169 and 181 non-redundant N-termini for *P. berghei* and *T. gondii*, respectively (Tables S1, S2 and Fig. S1A). The corresponding proteins were found to be derived from several compartments, with most being from the cytosol, nucleus, mitochondria, ER and the post-Golgi secretory pathway (including rhoptries, micronemes and dense granules; Sheiner and Soldati-Favre, 2008). The functions associated with the identified proteins include protein synthesis, proteostasis (chaperones and proteolysis), the cytoskeleton (actin and myosins), glycolysis, the Krebs cycle and DNA-binding proteins, including histones and the specific apicomplexan machinery (see protein descriptions, Gene Ontology terms and subcellular location annotations in sheet number 4 of Tables S1 and S2). The data showed that N-terminal methionine excision (NME) occurs in apicomplexans with a specificity similar to that reported in other eukaryotes (Fig. 1A). NME was found to be slightly more frequent in *T. gondii* than in *P. berghei* (Fig. 1A), which is probably due to differences in codon usage between the two species. In contrast, the frequency of NTA was found to be lower in *T. gondii* compared to *P. berghei* (67% versus 82% of quantified N-terminal peptides; Tables S1 and S2). However, NTA is associated with similar specificities in both organisms (Fig. 1B), with Met, Ser and Ala N-termini being almost systematically N-α acetylated (NTAed; see sheet no. 4 in Tables S1 and S2). In addition, quantitative analysis showed that NTAed proteins have high average acetylation yields of 96±1% and 93±1% (mean±s.e.m.) in *P. berghei* and *T. gondii*, respectively. NTA in apicomplexan parasites appears to follow the rules of acetylation identified in other eukaryotes, with substrates mostly arising from the activity of the major enzymatic complexes. This includes the NatA complex, which is specific for N-termini exposed by NME, and NatB, NatC and NatE, which modify proteins retaining an N-terminal Met (Fig. 1C). Furthermore, NTA of histones H2A and H2B suggests the existence of an active NatD in *T. gondii*. The identification of NTAed actin peptides (DEEVQALVVD) is evidence for NatH unique activity on N-terminal acidic residues (see TGME49_209030 in Table S1, sheet no. 3). In *P. berghei*, the actin N-terminus was retrieved (GDEEVQALVI), acetylation of which does not appear to result from NatH activity but rather from NatA activity (PBANKA_1459300 in Table S2, sheet no. 3). We noticed that NatA activity is favored in *T. gondii*, similar to other eukaryotes (Fig. 1C; Fig. S1A and Table S1, sheet 6). In *P. berghei*, an unprecedented preference for NatB activity was noted; to our knowledge, this preference is unique and is in agreement with a reduced NME process in this organism (Fig. 1C; Fig. S1A and

Journal of Cell Science (2022) 135, jcs259811. doi:10.1242/jcs.259811

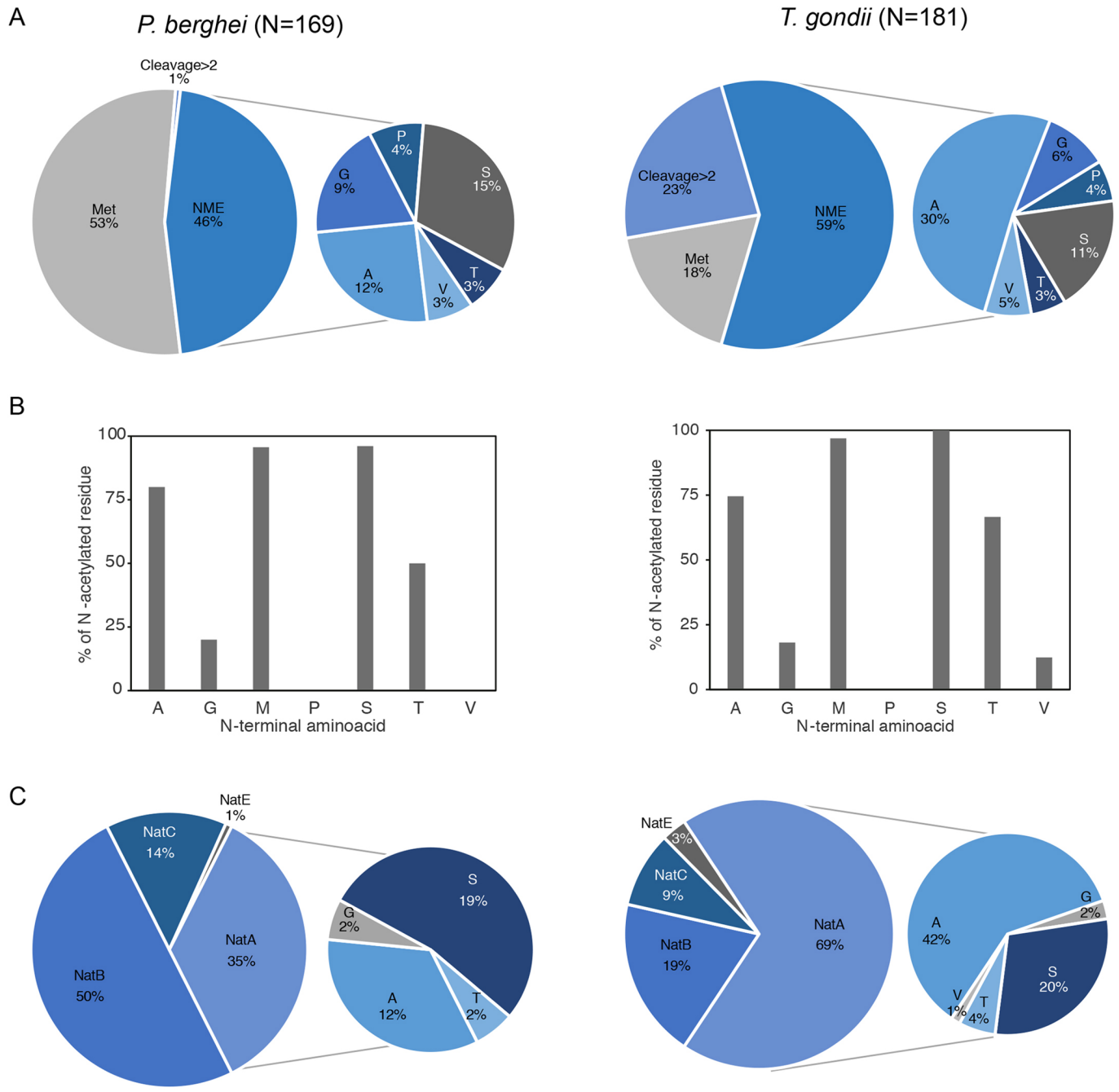

Fig. 1. Distinct N-terminal acetylation of *T. gondii* and *P. berghei* proteins. (A) Summary of NME in *P. berghei* (left) and *T. gondii* (right). For each species, the left-hand pie chart shows the percentages of N-termini identified as either the initiator methionine (Met), the product of NME, or the result of cleavage downstream of position 2 (cleavage>2); the right-hand pie chart shows a further breakdown of NME-derived N-termini based on amino acid residue. *N* values indicate the number of unique N-termini. (B) Percentage of the identified N-termini that were found to be acetylated, shown for each N-terminal residue in both *P. berghei* (left) and *T. gondii* (right). (C) Overview of NAT assigned substrate specificities. N-terminal acetylated substrates identified in *P. berghei* (left) or *T. gondii* (right) are classified based on the likely major active NAT responsible for the acetylation (left-hand pie charts), according to previously described classic NAT substrate distributions. Predicted NatA substrates are further categorized based on their N-terminal residues (right-hand pie charts).

Table S2). Our data also indicate that the N-termini of proteins of all major compartments of the parasites except the apicoplast could be identified. NTA is similar in all compartments retrieved, including the ER- and post-Golgi-located proteins of the secretory pathway (Table S3). Interestingly, *T. gondii* showed an unusually high level of NTAed proteins belonging to the secretory pathway.

We compared this newly generated *T. gondii* dataset with reanalyzed and unfiltered data from previous publications (Dogga et al., 2017; Coffey et al., 2018). This analysis revealed a strong correlation between changes on the N-termini amongst all three datasets (Table S1). Compilation of all these datasets yielded 696 non-redundant proteoforms with at least one N-terminal acetylated peptide. Among these, we identified 159 N-termini starting at the first Met and 318 N-termini starting at the second amino acid. The NME rules imposed by methionine aminopeptidase specificity (i.e. Met removal occurs when the side chain of the second residue is

Journal of Cell Science (2022) 135, jcs259811. doi:10.1242/jcs.259811

small, including for A, C, G, P, S, T, V) were found to be identical to those observed in other organisms (Martinez et al., 2008; Frottin et al., 2009, 2016). Filtering out downstream N-termini starting with a Met or having a Met at position −1, we additionally retrieved 87 N-termini (Table S1). These additional N-termini accurately matched the NME rules and thus strongly support that these correspond to the proper translation start site, allowing us to re-annotate the N-terminus of those proteins. Among the retrieved N-termini starting at position 1 or 2, we observed NTA of 161 N-termini, and for 88 of these we could quantify the yield of NTA (Table S1).

Interestingly, the analysis of the N-terminal acetylated peptides in the enlarged compiled dataset (Table S1) further confirmed the existence of *T. gondii* NATs with substrate specificity comparable to that observed for NatA, NatB, NatC and NatE in other organisms (Aksnes et al., 2016; Giglione and Meinnel, 2021). Similar results were obtained when we applied the SILProNAQ pipeline to *P. berghei* extracts (Table S2 and Fig. S1A). Accordingly, homologs of the catalytic subunits of the NatA–F complexes (NAA10, NAA20, NAA30, NAA40, NAA50 and NAA60, respectively) could be retrieved in the proteome of *T. gondii* (Table S4). Homologs of only NAA10, NAA20. NAA30 and NAA40 were identified in *P. berghei*, whereas NAA50 and NAA60 homologs were missing, as also appears to be the case in other *Plasmodium* species including *P. falciparum* (Rathore et al., 2016) (Table S4). We could identify a homolog of the auxiliary NAA15 subunit of the NatA complex in Apicomplexa but failed to identify the auxiliary subunit HypK (Table S4). We also identified a homolog of the NatB auxiliary subunit NAA25 in *T. gondii* but not in *Plasmodium* spp. (Table S4). Given that NAA25 has been shown to be required for NatB activity in yeast and mammalian cells (Van Damme et al., 2012), the absence of a clear NAA25 sequence homolog in *Plasmodium* spp. might mean that the NatB catalytic subunit in these organisms evolved to ensure the NatB function alone or that another non-homologous protein ensures the auxiliary function. Additionally, as for NatB, we could not identify homologs of NAA35 or NAA38, which are the auxiliary subunits of NatC, in both *T. gondii* and *P. berghei.* NatH (NAA80) homologs could not be identified in either of these apicomplexan species. Nevertheless, such activity does exist in *T. gondii*, as discussed above. Finally, the identified apicomplexan Nat catalytic subunit domains showed strong similarities to those of all other eukaryotes, including humans, with the exception of NAA30 (Fig. S2).

Acetylation of new N-termini originating from proteolytic cleavage along the secretory pathway in parasites

As reported above, our *T. gondii* N-terminal acetylome data features a high percentage of NTAed proteins. In total, 23% of the NTAed proteins (41 unique entries; Fig. 1A) displayed an N-terminus starting well beyond the second amino acid, of which 14 displayed acetylation with a yield greater than 20%. From this list, we realized that ten of 42 entries needed to be discarded as they start with a Met or on a residue that is preceded by a Met, which fits with the NME rules (see above). Within the list of the NTAed peptides starting downstream of position 2, we identified six proteins in the secretory pathway (GRA1, GRA2, GRA7, GRA9, ROP9, SRS30C) for which NTA yield was always higher than 95%, when measurable. When the same filtering was applied to the qualitative and published N-acetylomes (Dogga et al., 2017; Coffey et al., 2015), in conjunction with our current quantitative data, 94 proteins were found to display both N-termini downstream of the N-terminal Met and doubtless NTA status (Table S1 and Fig. S1A). Of these, 31 proteins – including members of the GRA, MIC, RON, ROP and SRS protein families, as well as aminopeptidase N and aspartyl protease ASP5 – are well recognized to be associated with the secretory pathway and to undergo signal peptide and/or further proteolytic processing (Table S1, sheet no. 7; Coffey et al. 2015, 2018). We noticed that several of these proteins display multiple cleavage sites, either within vicinal residues next to a main proteolytic cleavage site or much beyond, with NTA associated with each site identified (Table S1 and Fig. S1A). This implies that NTA may occur all along the secretory pathway at the ER and results from several independent proteolytic cleavages starting with signal peptide removal (Fig. S1B). As proteolytic processing of these proteins has already been reported to occur in the ER, we concluded that an NTA machinery is likely associated with the ER. The substrate specificity of the NAT involved in this machinery appears similar to that of a NatA, as it modifies mostly small residues: A, G, S, T or V. The associated number of such proteins is as high as for cytosolic proteins. However, unusual N-terminal residues – including L, K and H – were also found to undergo NTA, but quantification was not possible for any of these modifications, preventing a conclusion about the efficiency of this NTA. This unusual substrate specificity is very similar to that of plastid GCN5-related N-acetyltransferases (GNATs) of plants, which act on plastid-imported proteins after cleavage of the transit peptide (Giglione and Meinnel, 2021; Bienvenut et al., 2020); however, no such plastid GNAT homologs could be identified in apicomplexan proteomes. The low frequency of processed proteins in *P. berghei* (three proteins) prevented us from concluding whether *Plasmodium* spp. also display such machinery. We cannot exclude that ER NTA is associated with later differentiated states of the parasite or with different interactions with the host.

Taken together, the data suggest the occurrence of an N-terminal acetylation machinery located in the ER of apicomplexan parasites that has specificity corresponding mainly to a NatA but that also encompasses NatB activity, based on the frequency of the retrieved amino acids (A≫G, M, S, T or V).

T. gondii encodes multiple acetyltransferases that localize to various subcellular compartments

The data reported above suggest NTA activity in several compartments within apicomplexan parasites. Using sequences of known eukaryotic NATs of the GNAT family, we performed genome searches in ToxoDB.org and PlasmoDB.org and obtained 15 putative acetyltransferase enzymes in *T. gondii*, as reported previously (Cova et al., 2018), with 7 out of 15 matching previously characterized human NAT enzymes (Table S4). In addition, we examined previously reported predictions of the contribution of each putative enzyme to the fitness of *T. gondii* tachyzoites, based on a genome-wide CRISPR-Cas9 screen (Sidik et al., 2016); blood-stage *P. berghei*, based on detection of barcoded mutants (Bushell et al., 2017); and blood-stage *P. falciparum*, based on the results of transposon mutagenesis (Zhang et al., 2018) (Table S4). The subcellular localization of some of these proteins has also been predicted by hyperplexed localization of organelle proteins by isotopic tagging (hyperLOPIT) analysis (Table S4) (Barylyuk et al., 2020).

Because of an unusual primary protein structure featuring long N-terminal extensions before the predicted C-terminal acetyltransferase domain that could influence subcellular localization and drive the proteins to the ER, we focused on three genes encoding *T. gondii* homologs of the conserved GNAT machinery for further investigation of the ER acetylation machinery (Fig. S3A): TGME49_259070, which encodes the putative catalytic

Journal of Cell Science (2022) 135, jcs259811. doi:10.1242/jcs.259811

NAA30 subunit of NatC (named TgNAA30); TGME49_305450, which encodes a putative NAT8 enzyme (here named TgNAT8) – an ER-resident protein N-acetyltransferase (Ko and Puglielli, 2009; Mak et al., 2014); and TGME49_221160, which encodes a putative NAT with no known homologs (named TgNAT) (Table S4, Fig. S3A). The three selected putative NATs are predicted to contribute to tachyzoite stage fitness based on their negative fitness scores (TgNAA30, −2.51; TgNAT, −1.69; TgNAT8, −1.32), and all three proteins bear the conserved catalytic acetyltransferase GNAT domain (Fig. S3B). TgNAT8 is predicted to occupy similar subcellular localization as its human homolog, whereas localization information is not available for TgNAT and TgNAA30 (Table S4). TgNAT8 is conserved in all apicomplexans, whereas TgNAA30 is present in Coccidia and Haemosporida, and TgNAT is specific to coccidians (Fig. S3A). We identified that TgNAT8 has an NTAed terminus located at Ala2 (Table S1, sheet 4), which is compatible with its expression in *T. gondii* with a cytosolic N-terminal side and the GNAT domain within the ER guided by the single transmembrane (TM) domain (Fig. S3B).

To study the function of these three enzymes, protein degradation elements – mini auxin-induced degron (mAID) coupled to three Ty epitope tags (2885 nucleotides) – were fused to the C termini of TgNAT8 (to give NAT8mAID–Ty) and TgNAA30 (to give NAA30mAID–Ty) in parasites expressing the plant auxin (IAA) reporter TIR1 (Brown et al., 2018) (Fig. S3C). Several attempts at fusing the mAID–3×Ty construct at the C terminus of TgNAT were unsuccessful, plausibly due to its bulk, hence a smaller DiCre-driven U1 pre-mRNA degradation sequence fused to three Ty epitope tags (2473 nucleotides) was inserted at the C terminus in the endogenous TgNAT locus (to give NAT–U1–DiCre–Ty; Pieperhoff et al., 2015) (Fig. S3D). These strategies allowed the localization as well as the conditional depletion of the proteins upon addition of IAA (for mAID degradation) or rapamycin (for U1 degradation). Localization of TgNAA30, TgNAT8 and TgNAT was established using an immunofluorescence assay. NAA30mAID–Ty exhibited a granulated cytosolic appearance, matching the cytosolic localization of its homologs (Fig. 2A). NAT8mAID–Ty exhibited a perinuclear, residual body and cytosolic presence, which is representative of the parasite ER localization (Fig. 2A). NAT–U1–DiCre–Ty was confined to the parasite nucleus and colocalized with the nuclear DNA marker DAPI (Fig. 2A). Addition of IAA led to downregulation of TgNAA30 and TgNAT8. Western blots of extracellular parasites with or without IAA treatment showed NAA30mAID–Ty and NAT8mAID–Ty to migrate between the 70 and 100 kDa mass markers – their predicted molecular masses are 52 kDa and 57 kDa, respectively – with subsequent protein loss upon treatment with IAA (Fig. 2B). Downregulation of TgNAA30 did not affect parasite development, as assessed by plaque formation 7 d post infection of confluent human foreskin fibroblasts (HFFs) (Fig. 2C,D; P=0.2619 for −IAA, P=0.9911 for +IAA). Examination of the intracellular growth of parasites treated or not with IAA for 24 h showed that downregulation of TgNAA30 did not influence parasite replication (Fig. 2E). Depletion of TgNAT8 upon addition of IAA led to a minor but non-significant impact on intracellular growth (Fig. 2E). Concordantly, a slight change in plaque formation was observed upon treatment of NAT8mAID–Ty parasites (P=0.3187 for −IAA, P=0.0593 for +IAA) (Fig. 2C,D).

AT1 is conserved in apicomplexan parasites

Among all identified candidates, the NAT8 homolog TgNAT8 might display physiological function compatible with protein acetylation in the ER, when taking in account its localization and effects on parasite fitness. In addition, although NAT8 has previously been shown to acetylate lysine side chains, it is possible that this protein, as is the case for the recently characterized plastid GNATs, might display dual K-acetylation and NTA activities. Because modification of the ER-localized TgNAT8 induced parasite development defects, we surmised that perturbation of any member of the ER acetylation machinery, particularly ER-localized AT1 might dramatically affect protein acetylation in the ER. As NATs and NAT8 rely on acetyl-CoA, we challenged the origin of this compound in the ER. Mammalian AT1 translocates acetyl-CoA into the ER lumen (Jonas et al., 2010), whereas *Plasmodium* and *T. gondii* have an intricate acetyl-CoA synthesis and utilization network (Fig. 3A). Therefore, we investigated the impact of deletion of the ER acetyl-CoA transporter AT1 on parasite fitness and its link to ER protein acetylation.

Mammalian AT1 sequences are highly similar, and the human AT1 is predicted to contain a leucine zipper motif and multiple TM domains (Hirabayashi et al., 2013). AT1 is present in Coccidia, Haemosporida and Cryptosporidiidae but appears to be missing in Chromerida, Gregarinasina and Piroplasmida (Fig. 3B). *T. gondii* encodes only one putative AT1 homolog, TgAT1 (encoded by *TGGT1_215940*). TgAT1 localization to the ER has been predicted by hyperLOPIT analysis and subsequently confirmed by epitope tagging (Barylyuk et al., 2020; Tymoshenko et al., 2015) (Fig. 3B). The protein contains 605 amino acids with nine predicted TM domains and a signal peptide at the N-terminus (Fig. 3C). The *P. berghei* AT1 homolog, PbAT1, is encoded by *PBANKA_0519800* and shares 30.5% amino acid sequence identity with TgAT1 (Fig. S4A). PbAT1 is expressed in both erythrocytic asexual and sexual stages and with a peak of expression at the schizont stage (Fig. S4B,C). The protein contains 557 amino acids with 12 predicted TM domains and a coiled-coil domain (Fig. 3C). PbAT1 and TgAT1 bear little similarity to the human AT1 sequence, sharing 28.9% and 31.1%, sequence identity, respectively (Fig. S4A), which might reflect divergent evolution with an unknown bearing on functional roles.

PbAT1 is important for erythrocytic proliferation of *P. berghei*

In a large-scale signature-tagged mutagenesis study, deletion of Pb*AT1* was previously reported to reduce growth of the asexual blood stage (Bushell et al., 2017; Stanway et al., 2019). To further investigate the requirements for PbAT1 in erythrocytic proliferation and in the *Plasmodium* life cycle (Fig. S4C,D), its encoding gene was deleted using the PlasmoGEM knockout vector PbGEM_265292 (Fig. S4E,F) in the 820cl1mfcl1 clone to produce 820cl1Pb*AT1-KO* to facilitate the phenotyping of sexual stages (Fig. S4G). This line expresses green fluorescent protein (GFP) and red fluorescent protein (RFP) under the control of male- and female-specific promoters, respectively (Mair et al., 2010). An independent Pb*AT1-KO* clonal line was generated in the 2.34 parental strain to produce 2.34Pb*AT1-KO* (Fig. S4G), and this line was used for assaying the Pb*AT1* deletion phenotype by immunofluorescence.

The 820cl1Pb*AT1-KO* line showed a 14-fold reduction (P=0.0002) in parasitemia compared to the 820cl1mfcl1 mother line 6 d after the intraperitoneal injection of ∼50,000 parasites (Fig. 3E). To confirm this severe growth phenotype, we investigated the relative growth of 820cl1Pb*AT1-KO* compared with the 2.34 parental line in a competition assay where a 5:1 ratio of 820cl1Pb*AT1-KO* to wild-type 2.34 parasites were simultaneously injected. The kinetics of 820cl1Pb*AT1-KO* and 2.34 parasite growth were measured over 6 d using flow cytometry, where 820cl1Pb*AT1-*

Journal of Cell Science (2022) 135, jcs259811. doi:10.1242/jcs.259811

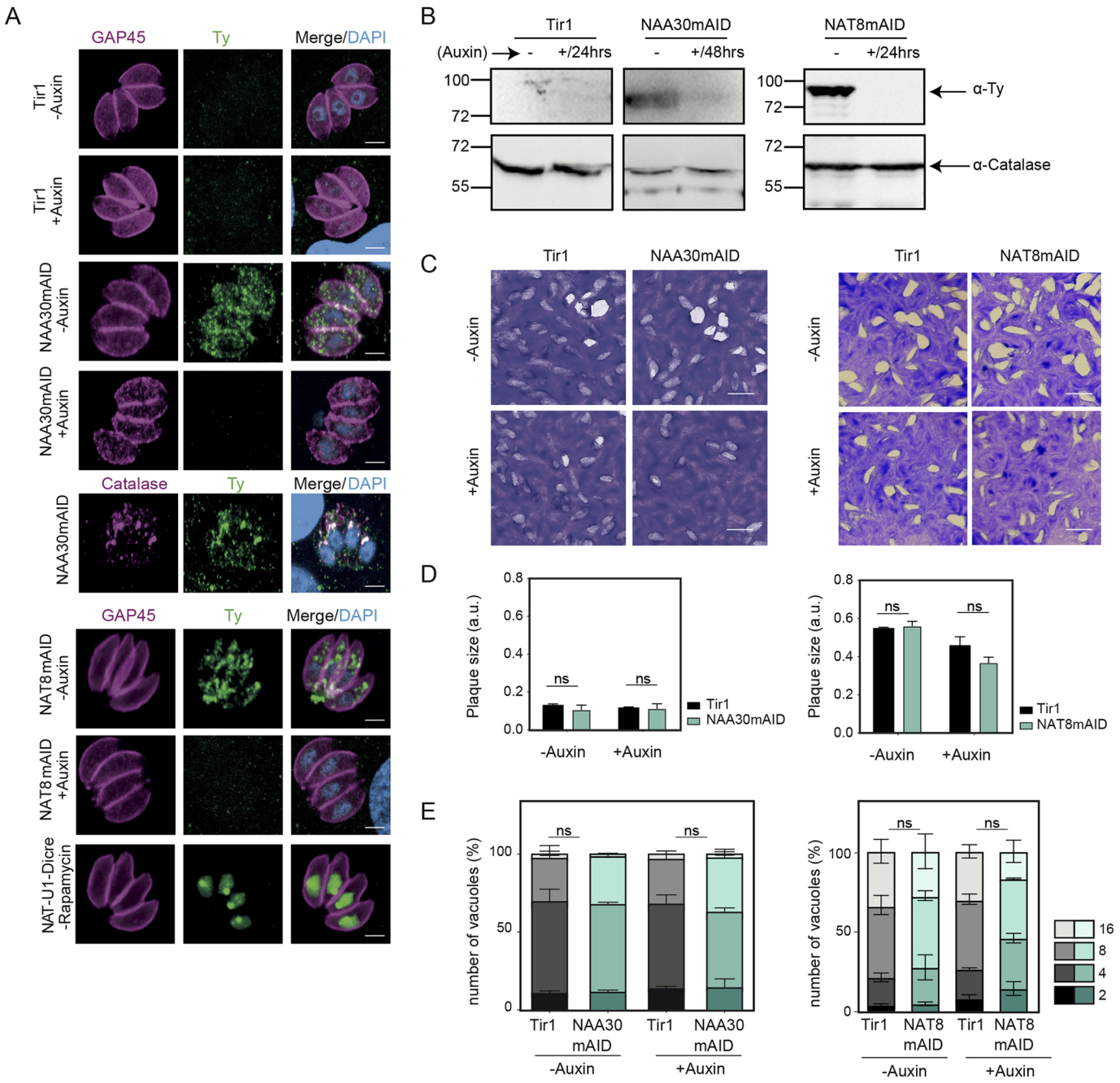

Fig. 2. Putative GNAT acetyltransferases localize to the ER and nucleo-cytosol compartments of *T. gondii*. (A) Immunofluorescence assays carried out using an anti-Ty antibody (green) and antibodies to detect either the parasite periphery marker GAP45 (magenta) or the cytosolic protein catalase (magenta) in endogenously tagged NAA30mAID–Ty and NAT8mAID–Ty *T. gondii* parasites, and in the control strain (Tir1), under conditions with (+Auxin) or without (−Auxin) IAA. Nuclei are stained using DAPI (blue). NAA30mAID–Ty localizes to the cytosol and partially colocalizes with catalase. NAT8mAID–Ty exhibits ER-like localization. Loss of Ty signal is observed for both NAA30mAID–Ty and NAT8mAID–Ty in the presence of IAA. The bottom row shows immunofluorescence assays carried out as described above using NAT–U1–Dicre–Ty *T. gondii* parasites in the absence of rapamycin. NAT–U1–Dicre–Ty localizes to the nucleus. Images are representative of three independent experiments. Scale bars: 2 µm. (B) Immunoblots showing migration of TgNAT8 (NAT8mAID–Ty) and TgNAA30 (NAA30mAID–Ty) proteins between 70 and 100 kDa in the absence of IAA (−Auxin), as detected using an anti-Ty antibody. Positive regulation of proteins is indicated by loss of the anti-Ty signal upon addition of the protein degradation inducer IAA (+Auxin) for the indicated times. The control Tir1 strain is shown as a negative control, and catalase is shown as a positive control. Blots shown are representative of three independent experiments. (C) Plaque assays of NAA30mAID–Ty and NAT8mAID–Ty parasites compared to control parasites (Tir1) at 7 d post infection of confluent HFFs in the presence (+Auxin) or absence (−Auxin) of IAA. HFFs were stained with Crystal Violet. Scale bars: 5 µm. (D) Quantification of plaque size, assays as described in C. Mean±s.d. of three independent experiments. ns, not significant (two-tailed unpaired Student's *t*-test). (E) Intracellular growth of NAA30mAID–Ty and NAT8mAID–Ty *T. gondii* compared to that of the Tir1 control strain. HFFs were infected with parasites under +Auxin and −Auxin conditions, as indicated, and examined 24 h post infection. Number of parasites per vacuole was enumerated and used to categorize the vacuoles based on parasite number (see key in figure: left, Tir1; right, NAA30 and NAT8). Stacked bar graphs show the percentage of vacuoles in each category. A defect in replication is observed in NAT8mAID–Ty parasites. Results are means±s.d. of three independent experiments. ns, not significant (two-tailed unpaired Student's *t*-test).

Journal of Cell Science (2022) 135, jcs259811. doi:10.1242/jcs.259811

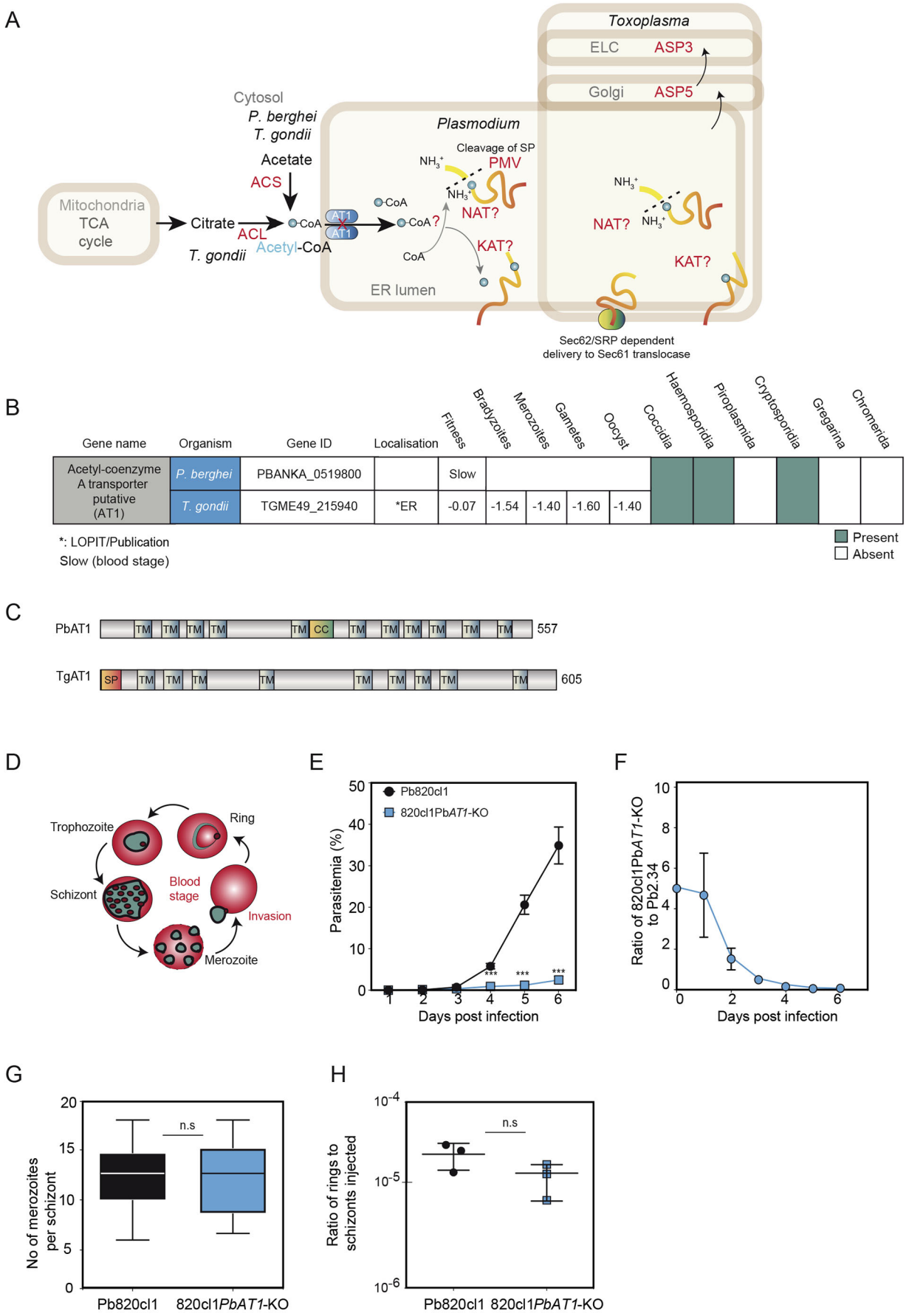

Fig. 3. See next page for legend.

Journal of Cell Science (2022) 135, jcs259811. doi:10.1242/jcs.259811

Fig. 3. AT1 is a fitness determinant of *P. berghei* erythrocytic forms. (A) Schematic illustration of acetyl-CoA synthesis in the cytosol of *T. gondii* and *P. berghei* by acetyl-CoA synthetase (ACS) and ATP citrate lyase (ACL) enzymes. The presence of AT1 on the ER membrane and the presumed role of AT1 in import of acetyl-CoA into the ER lumen are indicated. Cleavage of peptides by *Plasmodium* plasmepsin V (PMV) and acetylation by unknown NATs and KATs (including NAT8) in the ER lumen is shown. Aspartyl protease 5 (ASP5) and aspartyl protease 3 (ASP3) cleave proteins in the Golgi and endosomal-like compartment (ELC), respectively, in *T. gondii*. SP, signal peptide; SRP, signal recognition particle. (B) Summary of conservation of *T. gondii* and *P. berghei AT1* genes in the Apicomplexa phylum based on BLAST search using VEuPathDB (green, present; white, absent), expression of Tg*AT1* mRNA at different stages of *T. gondii* life cycle compared to tachyzoite stage (log_2 fold change), prediction of AT1 contribution to fitness for *T. gondii* based on a previous genome-wide CRISPR-Cas9 fitness screen (Sidik et al., 2016) and for *P. berghei* based on a previous genome-wide knockout screen (slow growth at blood stage; Bushell et al., 2017), and localization of AT1 in *T. gondii* based on hyperLOPIT (Barylyuk et al., 2020). (C) Graphic of PbAT1 and TgAT1 proteins, indicating amino acid length and putative domains (CC, coiled-coil domain; SP, signal peptide). (D) Illustration of the steps in the *Plasmodium* blood stage cycle. (E) Marked low parasitemia in mice infected with 820cl1Pb*AT1*-KO parasites compared to that in mice infected with wild-type parasites (Pb820cl1) measured by flow cytometry and presented as percentage parasitemia. *N*=5 mice per group. Data are presented as mean±s.d. ***P<0.001 (two-tailed paired *t*-test). (F) 820cl1Pb*AT1*-KO parasites are outgrown by wild-type Pb2.34 parasites *in vivo* during a parasite growth competition assessment by flow cytometry with a starting 820cl1Pb*AT1*-KO to wild-type ratio of 5:1. *N*=5 mice per group. Data presented as mean±s.d. (G) A comparable number of merozoites per schizont in wild-type and 820cl1Pb*AT1*-KO parasites was counted from purified schizonts, indicating normal development during the blood stage cycle (100 schizonts counted per experiment, *n*=3). Box and whisker plots show the median (line), interquartile range (box) and minimum and maximum values (whiskers). n.s., not significant P>0.05 (two-tailed paired *t*-test). (H) Fewer rings were detected post infection of mice with equal numbers of wild-type and 820cl1Pb*AT1*-KO schizonts. Data are presented as mean±s.d. of *n*=3 mice. n.s., not significant P>0.05 (two-tailed paired *t*-test).

KO parasites were detected by the expression of GFP and RFP, and 2.34 parasites were detected by Hoechst staining. The 820cl1Pb*AT1-KO* line was outcompeted by 2.34 parasites in less than 5 d post infection (Fig. 3F). Proliferation of asexual blood stages involves the invasion of new RBCs by the merozoite forms upon rupture of infected RBCs by mature schizonts (Fig. 3D). Following a 16 h *in vitro* culture, 820cl1Pb*AT1-KO* ring and trophozoite stages formed microscopically normal schizonts with a number of merozoites comparable to those of 820cl1mfcl1 parasites (P=0.6068) (Fig. 3G). To test whether the resulting merozoites were infective, blood containing ∼50,000 820cl1Pb*AT1-KO* and 820cl1mfcl1 schizonts was injected intravenously in naïve mice, and the ring parasitemia was determined 1 h post injection by blood smear followed by microscopy. A similar number of circulating ring forms were detected in the 820cl1Pb*AT1-KO* and control groups (P=0.1695) (Fig. 3H). Presently, the lack of availability of a continuous culture system for *P. berghei* asexual blood stages limits the dissection of the entire RBC cycle *in vitro*. Furthermore, examining these steps *in vivo* is technically challenging. Despite this, we have validated the findings that PbAT1 is crucial for proliferation *in vivo*.

PbAT1 is essential for the sexual development of *P. berghei*

Pb*AT1* was previously predicted to be essential for parasite transmission to the mosquito (Stanway et al., 2019) (Fig. S4D). Transmission of *Plasmodium* parasites to the mosquito initially relies on an irreversible pre-commitment of a few asexual stage parasites into female gametocytes (macrogametocytes) or male gametocytes (microgametocytes). As gametocytes of both sexes mature, they dramatically reduce their metabolic activity and become quiescent, waiting for uptake into the mosquito during a blood feed to resume their development. In 820cl1Pb*AT1-KO* parasites, an average of 0.6% male gametocytemia, compared to 1.32% for the parental line, was observed on day 3 following infection. Nearly no macrogametocytes could be detected in the 820cl1Pb*AT1-KO* line, with an average of 0.07% of cells being identified as macrogametocytes compared to 1.71% of cells in wild-type parasites, resulting in an altered sex ratio (Fig. 4A). The male gametocytes of the 820cl1Pb*AT1-KO* line also appeared to be empty and morphologically different from those of the wild-type line upon Giemsa staining (Fig. 4B). The findings therefore point to a role of PbAT1 during gametocytogenesis or sex determination.

We then investigated whether Pb*AT1-KO* microgametocytes were further able to form microgametes. Shortly after ingestion by a mosquito, microgametocytes undergo rapid gametogenesis at a permissive temperature in the presence of xanthurenic acid, a small molecule present in the mosquito midgut (Billker et al., 1998). In about 10 min, the haploid male gametocyte completes three rounds of genome replication and closed endomitosis, assembles the component parts of eight axonemes and, following nuclear division, produces eight flagellated motile male gametes in a process called exflagellation. At 10 min post activation, only 30% of the 820cl1Pb*AT1-KO* microgametocytes had attained octoploid status, compared to 90% of the wild-type group. We observed that 40% of the 820cl1Pb*AT1-KO* microgametocytes remained haploid despite activation, while the remaining 20% and 10% attained diploid and tetraploid status, respectively (Fig. 4C). Subsequent investigation after activation of 2.34Pb*AT1-KO* microgametocytes using immunofluorescence imaging also revealed a defect in axoneme assembly and the absence of egress from the RBCs (Fig. 4D,E). As a result, no active exflagellation centers were formed by 2.34Pb*AT1-KO* microgametocytes (Fig. 4F; P=0.0041). Taken together, these findings suggest that PbAT1 plays a critical function in female and male gametocytogenesis associated with defective microgametogenesis in *P. berghei*.

TgAT1 is important for the lytic stages of *T. gondii*

To delete Tg*AT1*, CRISPR-Cas9-mediated gene replacement with a drug selection cassette approach was used in the RH strain (Fig. S4H), and transfectants were identified using genomic PCR (Fig. S4I). The resulting knockout strain, Tg*AT1-KO*, exhibited a significant defect in lytic cycle development, as assessed at 7 d post infection *in vitro* by measuring plaque size on HFFs, compared to that of the wild-type line (P<0.0001) (Fig. 5A,B). This defect in growth was confirmed through growth competition assays (Fig. 5C). Tg*AT1-KO* parasites also displayed a slower intracellular development (Fig. 5D), but invasion of host cells was not impaired (P=0.7207) (Fig. 5E). These findings were unexpected, given the previously determined fitness score of −0.07, which indicates dispensability (Sidik et al., 2016).

TgAT1-driven influx of acetyl-CoA into the ER does not impact N-terminal acetylation of *T. gondii* proteins

As all known NATs use acetyl-CoA as sole acetyl donor, it is expected that dramatic acetyl-CoA depletion resulting from *AT1* knockout might lead to a decrease in the NTA of such proteins. We, therefore, performed comparative N-terminomics analysis on Tg*AT1-KO* and wild-type *T. gondii* parasites. The complete unfiltered data yielded 1499 identified N-termini (793 in the combined wild-type samples and 706 in the Tg*AT1-KO* samples), including 200 non-redundant proteoforms (181 in wild-type samples and 143 in Tg*AT1-KO* samples). Out of this dataset, 140

Journal of Cell Science (2022) 135, jcs259811. doi:10.1242/jcs.259811

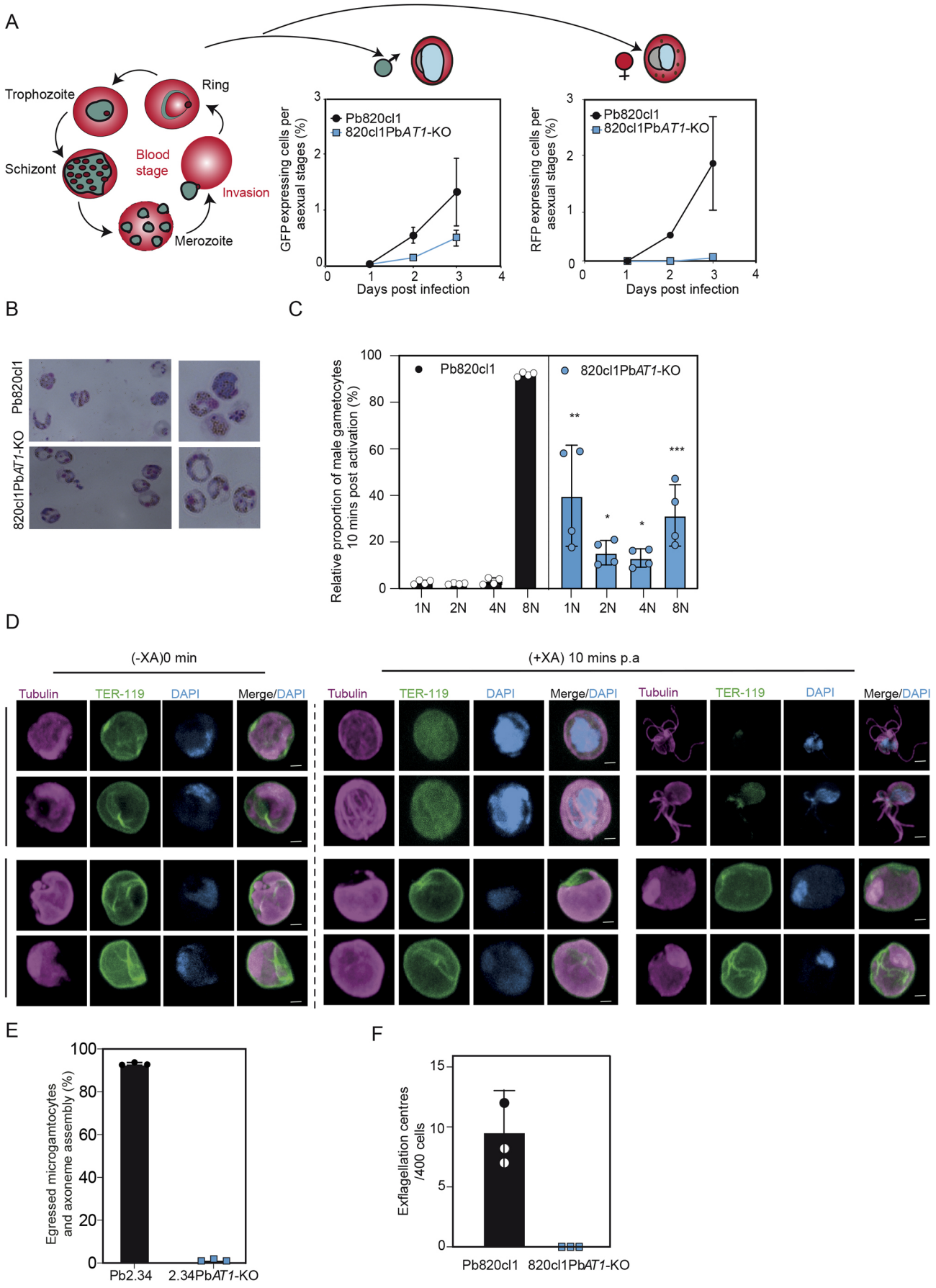

Fig. 4. See next page for legend.

Journal of Cell Science (2022) 135, jcs259811. doi:10.1242/jcs.259811

Fig. 4. Impaired gametocytogenesis and gametogenesis in the absence of *PbAT1*. (A) Left: illustration of the steps in the *Plasmodium* asexual blood stage cycle. Middle and right: flow cytometry measurements indicate fewer male microgametocytes (GFP-expressing cells, middle) and no female macrogametocytes (RFP-expressing cells, right) detected in 820cl1Pb*AT1*-KO compared to wild-type parasites (Pb820cl1) over the indicated period. Plots show the percentage of cells expressing GFP or RFP per asexual form, presented as mean±s.d. (n=4 mice). (B) Representative images of Giemsa-stained blood films of purified gametocytes, showing that 820cl1Pb*AT1*-KO male gametocytes appearing hollow compared to wild-type controls. Images are representative of four experiments. The width of an infected red blood cell is ∼10 µm. (C) Defective gametogenesis of male microgametocytes in the 820cl1Pb*AT1*-KO strain compared to the wild-type control. Ploidy of male gametocytes was assessed 10 min post activation with xanthurenic acid. Data are presented as mean±s.d. of n=4 experiments. *P<0.05; **P<0.01; ***P<0.001 (two-tailed paired t-test used). (D) Defective gametogenesis of male microgametocytes in the 2.34Pb*AT1*-KO strain, as compared to that of the wild-type Pb2.34 control, examined by immunofluorescence staining of α-tubulin (magenta) before (−XA, 0 min) and 10 min post activation with xanthurenic acid (+XA, 10 mins p.a.). The erythrocyte membrane marker TER-119 (green) was used to label RBCs, and DAPI (blue) was used to label DNA. DNA replication (middle panels), axoneme formation and egress from RBCs (right-hand panels) at 10 min post activation with XA were found to be absent in the 2.34Pb*AT1*-KO strain. Scale bars: 2 µm. Images are representative of two experiments. (E) Plot showing impaired gametogony in the 2.34Pb*AT1*-KO strain, as assessed by quantification of axoneme assembly and egress from RBCs observed by immunofluorescence (as shown in D). Data are presented as mean±s.d. (n=3). (F) 820cl1Pb*AT1*-KO cells do not form exflagellation centers, measured as motile active gametocytes at 15 min post activation with xanthurenic acid. Data are presented as mean±s.d. (n=3) P<0.0001 for AT1-KO vs control (E,F; two-tailed unpaired Student's t-test).

unique N-termini were properly quantified (Fig. S1A). The data were plotted on an abundance graph to compare global acetylation between the two conditions (Fig. 6A). Overall, these data show no obvious decrease in NTA level in the Tg*AT1-KO* line. Next, we looked at the correlation between the NTA yield observed in the Tg*AT1-KO* line and that observed in the wild-type line for each proteoform, either considering the total set of proteins or making a distinction between proteins that were NTAed on the initiator Met, proteins that underwent NME and were NTAed at position 2, and proteins that were further processed and NTAed on amino acids downstream (Table S1). Again, we observed unmodified NTA yields in both conditions, regardless of the position of the modification or the nature of the modified residue. We conclude that deletion of Tg*AT1* has no impact on the N-terminal acetylomes of the cytosolic compartment and the ER compartment.

We also analyzed *P. berghei* NTA in samples that were enriched for gametocytes (72% gametocyte purity, 28% late trophozoites or schizonts), comparing the 2.34Pb*AT1-KO* deletion line with the 2.34 wild-type line. As in the case of *T. gondii* samples, no alteration of the N-terminal acetylome was observed in the 2.34Pb*AT1-KO* gametocytes compared to that of wild-type gametocytes (Fig. 6A). In addition, as could be anticipated from our earlier analysis of the wild-type data, the 2.34Pb*AT1-KO* mutant data did not provide any additional information on the impact of NTA on secreted proteins. This could be due to (1) the very low number of proteins detected with a remote N-terminus caused by proteolytic cleavage (four proteins) and (2) the absence of associated NTA of any of those proteins. All of these four proteins – ETRAMP (PBANKA_0201600), PSOP1 (PBANKA_0619200), SEP2 (PBANKA_0501100) and EXP2 (PBANKA_1334300) – display a signal peptide that is predicted to be cleaved. Among them, we observed that a secreted ookinete protein (ETRAMP, PBANKA_0619200) displays a signal peptide featuring two cleavage sites in close proximity (positions 17 and 21), which plausibly could mediate entry into the secretory pathway. None of the neo-N-termini were found to be N-acetylated. Nevertheless, newly formed N-termini of secreted proteins featuring NTA have been reported to occur in the ER of *P. falciparum* (Chang et al., 2008; Osborne et al., 2010).

Loss of TgAT1 modestly alters K-acetylation of only a few proteins

To complete our investigation of the potential impact of blocking putative import of cytosolic acetyl-CoA into the ER on acetylation of proteins, we probed the lysine acetylome of *T. gondii* parasites lacking AT1 and compared it with that of wild-type parasites using mass spectrometry (MS)-based label-free quantitative proteomic analyses. Of the 313 K-acetylation sites reproducibly quantified, which were spread across 200 different proteins (Table S5; Fig. 6B), three that were present on the same peptide of ribosomal protein RPS6 were found to be significantly hyperacetylated in the Tg*AT1-KO* strain compared to their acetylation in the wild-type strain. We also identified one K-acetylation site in phosphofructokinase PFKII and one in dehydrogenase E1 component family protein that were hyperacetylated in the knockout strain (greater than 2-fold increase and P<0.01) (Table S5; Fig. 6C). Conversely, six lysines carried by six different proteins (GRA2, trypsin domain containing protein, AP2 domain transcription factor AP2X-7, and three hypothetical proteins) were found to be hypoacetylated in the knockout strain compared to their acetylation levels in the wild-type strain (Table S5; Fig. 6C). We compared the subcellular localization of the differentially K-acetylated proteins, as assigned previously by hyperLOPIT analysis (Barylyuk et al., 2020), and their CRISPR-Cas9-based tachyzoite fitness prediction scores (Sidik et al., 2016). The hyperacetylated ribosomal protein RPS6, which is a 40S ribosome protein found in the cytosol, and the AP2 domain transcription factor AP2X-7 make significant contributions to tachyzoite development, based on fitness prediction scores of −4.58 and −3.39, respectively (Fig. 6C; Table S5). The other three proteins localize to different secretory organelles and the Golgi and are predicted to be dispensable for tachyzoite development (Fig. 6C; Table S5). These findings suggest that TgAT1 is not a major driver of K-acetylation.

DISCUSSION

Acetylation is a major modification of proteins. K-acetylation is known as a prominent post-translational modification in malaria parasites (Doerig et al., 2015), which is likely due to the frequent occurrence of lysine residues as a result of its AT-rich genome (Chanda et al., 2005; Gardner et al., 2002). NTA of proteins not only occurs co-translationally in the cytosol but also post-translationally at the Golgi and plastid (Giglione et al., 2015; Aksnes et al., 2019; Linster and Wirtz, 2018). NTA modification seems to be less frequent on ER translocated proteins and may be a modification inhibiting targeting of cytosolic proteins to the ER (Forte et al., 2011). In this report, we assigned, from both sequence identity and global substrate specificity analysis, most apicomplexan acetyltransferase catalytic subunits to their proper protein substrate specificity either in the cytosol (NatA–C and NatE), the nucleus (NatD) or the inner cytosol membrane network (NatF). We found that both parasites have an unusually high level of protein acetylation in the ER, and this process occurs at various stages along ER protein maturation (Fig. 3A and Fig. S1B). The role of the acetyltransferase(s) involved in both K-acetylation and NTA, as well as the acetyl-CoA supply within the ER, were addressed further.

The data suggest that the most likely candidate for ER protein acetylation is the NAT8 homolog, the only predicted ER-resident

Journal of Cell Science (2022) 135, jcs259811. doi:10.1242/jcs.259811

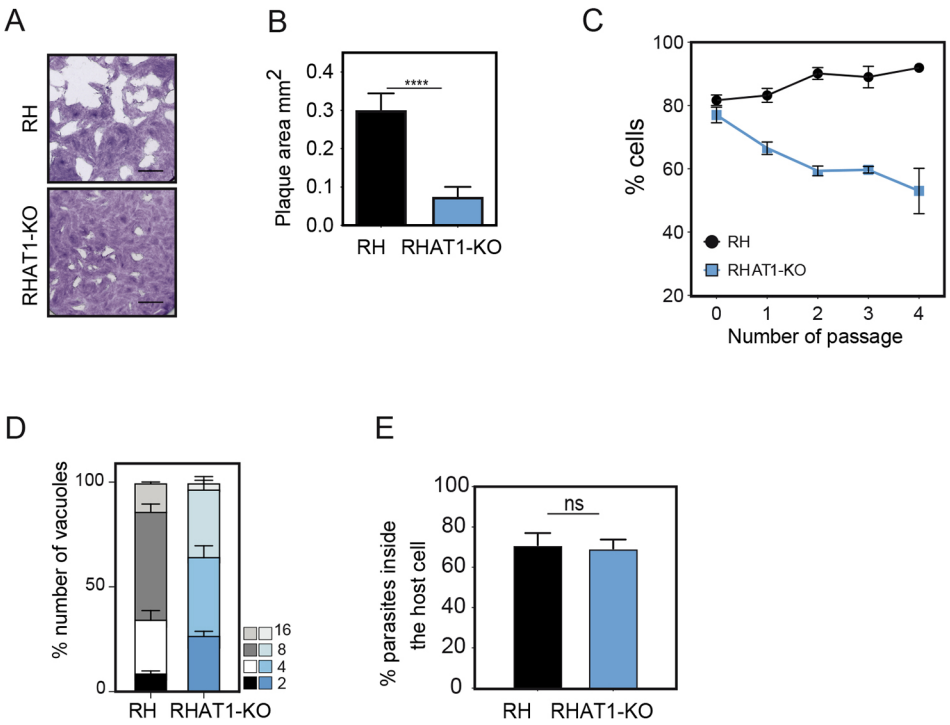

Fig. 5. AT1 is a fitness-conferring protein in *T. gondii* tachyzoite forms. (A) Plaque assay of Tg*AT1*-KO and wild-type control parasites (Tg) 7 d post infection of confluent HFFs, showing a severe defect in the lytic cycle of Tg*AT1-KO* parasites. HFFs were stained with Crystal Violet. Representative images of three independent experiments. Scale bars: 5 µm. (B) Quantification of plaque size assays as described in A. The Tg*AT1*-KO strain causes significantly smaller lytic plaques than those formed by the Tg control. Mean±s.d. of three independent experiments. ****P<0.00001 (two-tailed unpaired Student's *t*-test). (C) Flow cytometry-based assessment of Tg*AT1*-KO and Tg parasite growth in competition assays using GFP-expressing RH strain parasites as an internal control over four consecutive lytic cycles in HFFs validates the significant defect in Tg*AT1*-KO development. Data are presented as mean±s.e.m. of three independent experiments (two-tailed unpaired Student's *t*-test confirmed a difference between RH and RHAT1-KO). (D) Intracellular growth assay. HFFs were infected with Tg*AT1*-KO parasites and Tg controls. Immunofluorescence assays were performed using anti-GAP45 antibodies at 24 h, and the number of parasites per vacuole was enumerated and used to categorize the vacuoles based on parasite number (see key in figure). Stacked bar graphs show the percentage of vacuoles in each category. Slower intracellular growth of Tg*AT1*-KO parasites is observed compared to that of the wild type. Mean±s.d. of n=3 (two-tailed unpaired Student's *t*-test confirmed a difference between RH and RHAT1-KO). (E) Quantification of HFF invasion by Tg*AT1*-KO and Tg parasites. Tg*AT1*-KO parasites have a normal ability to invade HFFs. Mean±s.d. of three independent experiments. ns, not significant P>0.05 (two-tailed unpaired Student's *t*-test).

NAT in *T. gondii*. The TgNAT8 N-terminus was mapped in the course of our analysis and was shown to display an N-terminal acetylation on Ala2. This is a typical NatA (i.e. cytosolic) acetylation mark, and the absence of signal peptide cleavage further suggests that the N-terminus is most likely oriented towards the cytosolic side, as in mammals. With almost 300 residues, the disordered N-terminal cytosolic domain is, however, unusually large compared to that of mammalian NAT8 proteins (Farrugia and Puglielli, 2018; Ko and Puglielli, 2009) and its exact function is unknown. Like animal NAT8 proteins, TgNAT8 displays a single TM domain followed by the C-terminal GNAT acetyltransferase domain, which is located within the ER lumen. This domain relies on an acetyl-CoA fuel to promote protein acetylation in the ER. To date, NAT8 has been described as displaying lysine acetylase activity in mammals; nevertheless, as many studies now acknowledge, an increasing number of GNATs exhibiting both lysine acetylase and N-terminal acetyltransferase activities do exist (Bienvenut et al., 2020; Giglione and Meinnel, 2021; Meinnel et al., 2020). Therefore, one cannot exclude that TgNAT8 also displays N-terminal acetyltransferase activity. If TgNat8 is not responsible for the observed ER NAT activity, there are only four as-yet-unassigned GNAT homologs to propose as candidates (Table S4), and these proteins also represent candidate GNATs for *T. gondii* NatH activity, for which no direct homolog could be identified. Alternatively, one could envisage that free NAA10 or NAA20 subunits devoid of ancillary subunits might be translocated into the ER.

In mammals, AT1 activity is essential for cell viability and regulates cytosolic acetyl-CoA levels as well as K-acetylation of proteins in the secretory pathway, cytosol, nucleus and mitochondria (Dieterich et al., 2019; Jonas et al., 2010; Farrugia and Puglielli, 2018). Moreover, AT1 controls cell metabolism, including lipid metabolism and mitochondria bioenergetics (Dieterich et al., 2019). AT1 is the most relevant candidate to supply acetyl-CoA to the ER. However, we did not observe a correlation between AT1 inactivation and variations in the lysine and N-terminal acetylomes of ER-translocated proteins in Apicomplexa. This suggests the existence of an alternative source of acetyl-CoA supplying the ER in addition to that transported by AT1. This alternative source would be sufficient for the acetyltransferase catalyst(s) involved (e.g. NAT8) in the absence of AT1. In this context, alternative routes of acetyl-CoA import to the ER might occur through the nuclear pore and from the nucleus, through mitochondrion–ER (Mallo et al., 2021) or plastid–ER contact sites, or through acetyl-carnitine or acetyl-aspartate exchange. AT1 could therefore be involved in regulating the ER acetyl-CoA pool to increase its concentration above a minimal level that can otherwise be fulfilled by alternative processes. In support of this hypothesis, depletion of cytosolic acetyl-CoA in yeast has been shown to have no impact on global NTA of cytosolic proteins

Journal of Cell Science (2022) 135, jcs259811. doi:10.1242/jcs.259811

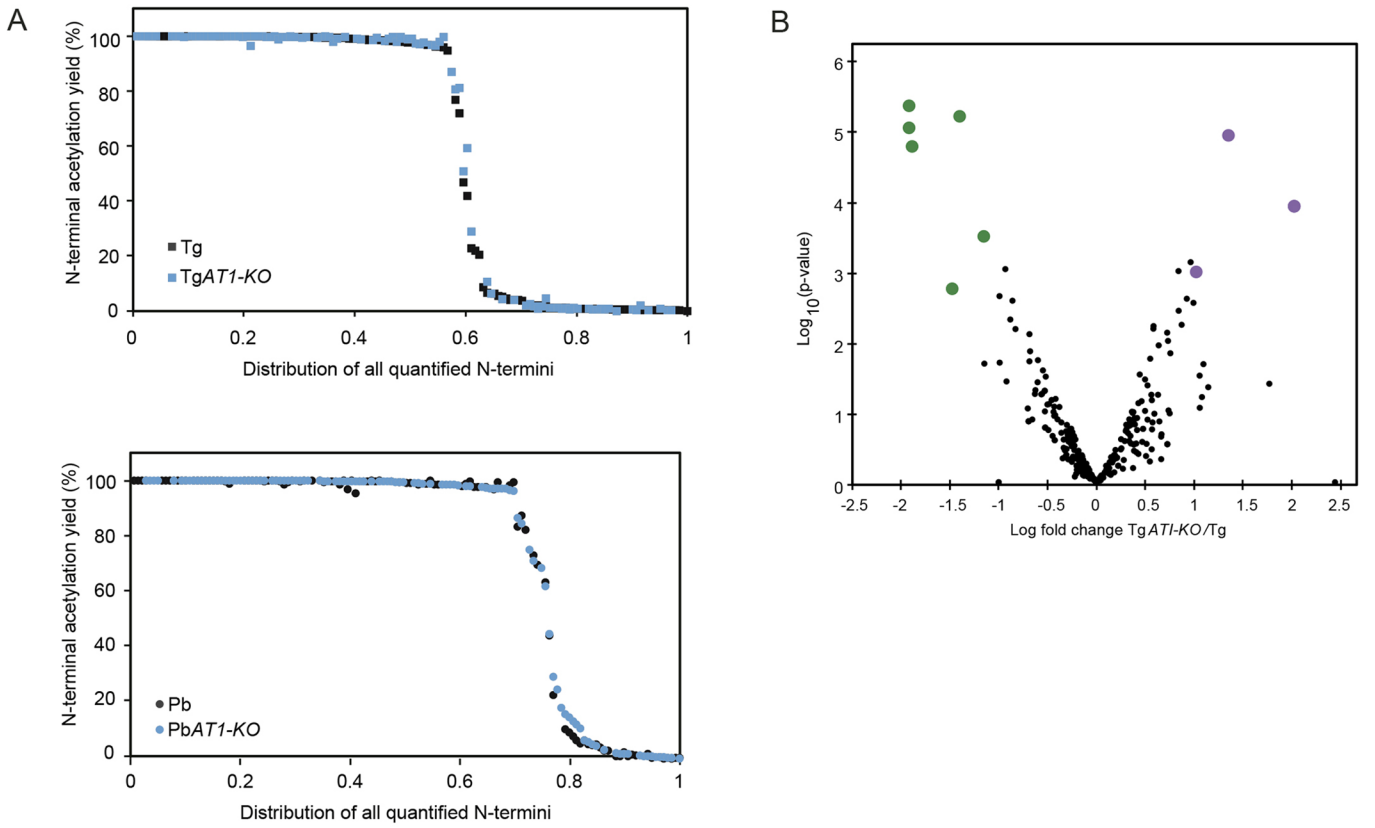

C

Gene name	Gene ID	Fitness	logFC (KO/WT)	Localization (LOPIT)	Bradyzoites	Merozoites	Gametes	Oocysts
ribosomal protein RPS6 (RPS6)	TGME49_210690	-4.58	2.01	40S ribosome	0.6	3.0	1.9	2.3
phosphofructokinase (PFKII)	TGME49_226960	-5.19	1.35	Cytosol	-1.7	1.6	1.7	2.0
dehydrogenase E1 component family protein	TGME49_239490	-1.89	1.02	Mitochondrion - soluble	-1.1	2.1	3.4	2.7
dense granule protein GRA2 (GRA2)	TGME49_227620	2.47	-1.91	Dense granules	-0.1	-582.5	-3052.9	-3052.9
AP2 domain transcription factor (AP2X-7)	TGME49_214840	-3.39	-1.40	nucleus - chromatin	-1.2	-4.5	-4.1	-3.5
trypsin domain-containing protein	TGME49_262920	0.56	-1.47	Rhoptries	0.1	-4.8	-8.7	-6.0
hypothetical protein	TGME49_216060	0.12	-1.15	Nucleus - chromatin	-1.3	-2.3	-3.0	-2.2
hypothetical protein	TGME49_271740	0.36	-1.88	Nucleus - non-chromatin	-1.2	-3.0	-3.2	-2.8
hypothetical protein	TGME49_212220	-4.91	-1.91	Golgi	-0.3	-1.1	1.1	1.1

Fig. 6. The *T. gondii* and *P. berghei* N-terminal acetylomes and *T. gondii* lysine acetylome are globally unaltered in AT1-knockout parasites. (A) Comparison of NTA yield of retrieved N-termini of proteins in Tg*AT1*-KO (top) and Pb*AT1*-KO (bottom) with the corresponding yields in wild-type parasites (Tg and Pb, respectively). N-termini are ranked by NTA yield. (B) Volcano plot comparing K-acetylation sites in Tg*AT1*-KO parasites and the Tg control strain. Statistically significant differences are determined as indicated in the Materials and Methods. Black, unchanged acetylation sites; purple, acetylation sites hyperacetylated in Tg*AT1*-KO; green, acetylation sites hypoacetylated in Tg*AT1*-KO (>2-fold change threshold, n=3). (C) Summary of proteins with hyperacetylated (blue) and hypoacetylated (green) K-acetylation sites in Tg*AT1*-KO, including their $\log_2$ fold change in acetylation (logFC KO/WT), hyperLOPIT predicted localization (Barylyuk et al., 2020), CRISPR-Cas9 fitness prediction (color gradient: blue, dispensable; red, essential; Sidik et al., 2016) and mRNA expression at different stages compared to tachyzoites [mRNA expression score corresponds to the $\log_2$ fold-change of the RNA-seq (transcriptomics reads) measured in different stages vs the tachyzoite stage].

(Varland et al., 2018; Cova et al., 2018). This suggests that ER acetyltransferases are effective at low acetyl-CoA concentrations (i.e. less than 5–25 µM, the average range of concentration in the cytosol; Pietrocola et al., 2015) and with K_m values of NATs in the same range (Farrugia and Puglielli, 2018). Our current data shows that AT1 is required for efficient growth in apicomplexans and that AT1 deletion has no apparent effect on acetylation of protein targets, which suggests a supplementary import activity of AT1 in addition to

Journal of Cell Science (2022) 135, jcs259811. doi:10.1242/jcs.259811

acetyl-CoA import for protein acetylation. Whether this is related to other, higher range (i.e. greater than C2) acyl-CoA import or to other small compounds is as yet unknown. Finally, as we identify few ER-resident targets but many post-Golgi targets, one cannot exclude that a transporter that is functionally similar to AT1 fuels secretory compartments downstream of the Golgi with acetyl-CoA. The very polarized secretory pathway of apicomplexan parasites required for cell invasion indeed mostly involves a directed vesicular flow downstream of the trans-Golgi network (Sheiner and Soldati-Favre, 2008).

P. falciparum exported and secreted proteins are also processed and acetylated in the ER (Chang et al., 2008; Osborne et al., 2010; this work). In *Plasmodium*, increase of acetate and/or acetyl-CoA in the cytosol specifically upregulates the K-acetylation status of acetyltransferases and of transcriptional, ribosomal and translation-related proteins, but it does not cause a generalized effect on the whole cellular lysine acetylome (Cobbold et al., 2016). This indicates that the ER acetyl-CoA pool is not limiting for protein acetylation in this compartment. The molecular mechanisms governing the specific metabolic requirements of female and male gametocytes in *Plasmodium* are elusive. Our results suggest a differential requirement for AT1 between females and males. Of interest are the nucleo-cytosol localized RNA/DNA binding ALBA proteins in *Plasmodium* spp. (Reddy et al., 2015; Vembar et al., 2015), whose functions are regulated by acetylation (Goyal et al., 2012). In *Plasmodium yoelii*, the absence of a member of the ALBA family (ALBA4) has been shown to be deleterious to the development of asexual forms and activation of male gametocytes (Muñoz et al., 2017). Proteome-wide K-acetylation analyses of this mutant might reveal substrates regulated by AT1 activity.

The different subcellular localization of the three investigated putative NATs in *T. gondii* aligns with the occurrence of NTA modifications in different compartments in eukaryotic cells (i.e. the cytosol, ER and nucleus). Nevertheless, unlike plants (Giglione and Meinnel, 2021), no plastid NAT could be identified in *T. gondii*. Deeper investigation of the NATs and characterization of N-termini in the absence of the identified acetyltransferases (Table S4) would be required to fully appreciate the functionality of NTA modifications in Apicomplexa.

MATERIALS AND METHODS

T. gondii parasite culture

T. gondii tachyzoites were grown in human foreskin fibroblasts (HFFs) purchased from American Type Culture Collection (ATCC; CRL-2088, CCD1072Sk). Dulbecco's Modified Eagle's Medium (DMEM, Gibco) supplemented with 5% fetal calf serum (FCS), 2 mM glutamine and 25 µg/ml gentamicin was used for maintenance of the cells. RHΔKu80 (referred to as Tg or RH; Fox et al., 2009), RHΔKu80-Tir1 (referred to as Tir1; Brown et al., 2018) and RH-DiCre (Pieperhoff et al., 2015) strains were used as parental strains for generation of mutants.

Cloning of DNA and generation of constructs

Parasite genomic DNA (gDNA) was extracted using the Wizard SV genomic DNA purification kit (Promega). PCRs were performed using Q5 (New England Biolabs), GoTaq (Promega) and KOD (Novagen) polymerases with primers listed in Table S6, according to the manufacturer's instructions. Cloning used *E. coli* XL-1 Gold chemo-competent bacteria.

Parasite transfection and selection of stable mutants

To generate a CRISPR-Cas9-directed Tg*AT1-KO* strain, PCR was performed using the Q5 site-directed mutagenesis kit on pSAG1::Cas9-U6::sgUPRT (Shen et al., 2014) vector as the template to produce double gRNA plasmid pSAG1::Cas9-U6::dgAT1 using primers 8723/8724, as previously described (Krishnan et al., 2020). A DHFR cassette was amplified by KOD PCR using 5′ and 3′ primers 8725/8726 that have 30 bp homology with the *AT1* gene upstream and downstream of the two gRNAs.

To produce NAA30mAID–Ty and NAT8mAID–Ty strains, KOD PCR was performed using primers 9994/9995 and 9984/9985 for NAA30 and NAT8, respectively, on vector pTub1-YFP:mAID:3Ty:DHFR:TS:HXGPRT, as described previously (Brown et al., 2018). NAT–U1–DiCre–Ty was generated using a KOD PCR product produced using primers 9991/9992 with vector pG152:KI:3Ty:Lox:SAG1:3UTR:HXGPRT.GB, as previously described (Pieperhoff et al., 2015). Single gRNAs for NAA30, NAT8 and NAT were produced by PCR using Q5 site-directed mutagenesis on pSAG1::Cas9-U6::sgUPRT using primers 9993/4883, 9983/4883 and 9998/4883 for NAA30, NAT8 and NAT, respectively, to generate pSAG1::Cas9-U6::sgNAA30, pSAG1::Cas9-U6::sgNAT8 and pSAG1::Cas9-U6::sgNAT. The PCR products were precipitated in using sodium acetate and ethanol and were resuspended in 100 µl of water prior to transfection. Co-transfections using 30 µg of the gene-specific gRNAs and respective KOD products in *T. gondii* tachyzoites were performed by electroporation, as previously described (Soldati and Boothroyd, 1993). Resistant parasites were selected with appropriate drugs, either mycophenolic acid (25 mg/ml) and xanthine (50 mg/ml) or pyrimethamine (1 µg/ml) for those carrying the HXGPRT (Donald et al., 1996) and DHFR cassettes (Donald and Roos, 1993), respectively. GoTaq PCR analyses were used to assess integration of the DHFR cassette using primer pairs 8727/2017 for 5′, 8728/2018 for 3′ and deletion of *AT1* using 8727/8728. The NAA30mAID–Ty, NAT8mAID–Ty and NAT–U1–DiCre–Ty strains were confirmed by immunofluorescence assays and western blot assays upon induction of protein degradation with 1 mM auxin (IAA) dissolved in ethanol or rapamycin (Sigma), as appropriate. All primer sequences are listed in Table S6.

Ethics statement

Experiments in mice were conducted under license number GE-30-13, according to the guidelines and regulations issued by the Swiss Federal Veterinary Office.

P. berghei maintenance, purification and transfection

Maintenance and transfections in *P. berghei* were performed as previously described (Balestra et al., 2020). Briefly, *P. berghei* ANKA strain (Vincke and Lips, 1948), derived clones 2.34 (Billker et al., 2004), 820cl1 (Mair et al., 2010) and Pb*AT1-KO* parasites were grown and maintained in 6–10-week-old female CD1 outbred mice. The mice were housed in rooms kept at 21±2°C under a 12 h light–dark cycle. They were kept in individually ventilated cages and fed commercially prepared autoclaved dry rodent meals and water provided as often as necessary. Regular screenings were carried out on the mice to ensure a pathogen-free status. Microscopy on methanol-fixed, thin blood smears stained with Giemsa was done to determine parasitemia of infected mice (Moll et al., 2013). Gametocyte production was enhanced by treatment of mice with phenylhydrazine (intra-peritoneal injection of 150 ml of 6 mg/ml phenylhydrazine resuspended in sterile PBS) 3 d prior to infection, followed by sulfadiazine (20 mg/l) treatment in drinking water 1 d post infection to clear the asexual forms. Exflagellation of male gametocytes was assessed on day 3 or 4 post infection by adding 4 µl of blood collected from a superficial tail vein to 70 µl exflagellation medium [RPMI 1640 containing 25 mM HEPES, 4 mM sodium bicarbonate, 5% fetal calf serum (FCS), 100 µM xanthurenic acid, pH 7.4]. Exflagellation centers were enumerated per 100 microgametocytes, and the percentage of RBCs infected with microgametocytes was assessed on Giemsa-stained smears. Gametocyte purification was performed by adding collected parasites to suspended animation medium (SA; RPMI 1640 containing 25 mM HEPES, 5% FCS, 4 mM sodium bicarbonate, pH 7.2). This was followed by gradient separation from uninfected erythrocytes on a Histodenz (Sigma) solution made from 48% of a Histodenz stock (27.6% w/v Histodenz in 5.0 mM Tris-HCl, 3.0 mM KCl, 0.3 mM EDTA, pH 7.2) and 52% SA, final pH 7.2, and collection of gametocytes from the interface.

To delete Pb*AT1*, NotI digestion was used to release the DNA insert from the backbone of PlasmoGem *AT1* knockout vector number PbGEM-265292 (see https://plasmogem.umu.se/pbgem/) followed by ethanol precipitation of DNA. For transfections, parasites were collected from mice and grown

Journal of Cell Science (2022) 135, jcs259811. doi:10.1242/jcs.259811

overnight *in vitro*, the schizonts were then purified by the gradient method, using Histodenz solution made from 55% Histodenz stock and 45% phosphate-buffered saline (PBS). Schizonts were collected from the intermediate layer, centrifuged at 500 ***g*** for 3 min, resuspended in 25 µl Amaxa Basic Parasite Nucleofector solution (Lonza) containing 10–20 µg of DNA (knockout linear vector) dissolved in 10 µl H_2O.

Cells were electroporated using the FI-115 program of the Amaxa Nucleofector 4D. Transfected parasites were subsequently resuspended in 200 µl fresh erythrocytes and injected intraperitoneally into mice. Parasite selection was started 1 d post infection using 0.07 mg/ml pyrimethamine (Sigma) in the drinking water (~pH 4.5).

Genotyping was performed using primers GW2/QCR2 and GW2/GT to check for integration of the vector into the locus, and QCR1/QCR2 and 6516/6517 primers to check for the wild-type locus. Primers sequences used are listed in Table S6.

Antibodies

The following antibodies were used in this study: rabbit polyclonal anti-GAP45 (1:10,000) and mouse monoclonal anti-Ty (BB2; 1:10), which have been described previously (Frenal et al., 2014; Plattner et al., 2008); mouse anti-α-tubulin (1:1000; clone DM1A; Sigma-Aldrich, T6199); TER-119 monoclonal antibody (1:500; Thermo Fisher Scientific, 12-5921-82); and anti-catalase (1:2000, Ding et al., 2000). For immunofluorescence assays, Alexa Fluor 488, Alexa Fluor 594 or Alexa Fluor 680 conjugated to goat anti-mouse IgG or anti-rabbit IgG (Life Technologies) were used. For western blot analyses, secondary peroxidase-conjugated goat anti-rabbit IgG or anti-mouse IgG antibodies (Sigma) were used.

Indirect immunofluorescence assay

Confluent HFF cells seeded on cover slips in 24-well plates were inoculated with test *T. gondii* strains for 24 h. This was followed by fixation with 4% paraformaldehyde and 0.05% glutaraldehyde in PBS (PFA/GA) and neutralization in 0.1 M glycine in PBS for 3–5 min. Samples were then processed with appropriate antibodies as previously described (Plattner et al., 2008; Nyonda et al., 2020). Immunofluorescence assays using *P. berghei* gametocytes were performed as previously described (Balestra et al., 2021; Volkmann et al., 2012). Briefly, purified gametocytes were fixed with PFA/GA for 1 h. This was followed by permeabilization with 0.1% Triton X-100 in PBS for 10 min and a blocking step in 2% BSA in PBS for 2 h. Primary antibody staining using anti-α-tubulin and TER-119 (erythrocyte membrane marker) diluted 1:1000 in blocking buffer was followed by secondary antibody staining. Confocal images were acquired using a Zeiss LSM800 with Airyscan and an apochromat 63×/1.4 oil objective at the Bioimaging core facility of the Faculty of Medicine, University of Geneva. *Z*-stack sections were processed using the ImageJ software (NIH, Bethesda, MD).

Flow cytometry analysis on *P. berghei* gametocytes

The DNA content of male gametocytes was measured as previously described (Fang et al., 2017). Purified gametocytes were resuspended in 100 µl of SA medium, and activation was induced by adding 100 µl of modified exflagellation medium (RPMI 1640 containing 25 mM HEPES, 4 mM sodium bicarbonate, 5% FCS, 200 µM xanthurenic acid, pH 7.8). 800 µl of ice-cold PBS was rapidly added to the cells to inhibit gametogenesis, and cells were stained for 30 min at 4°C with Vybrant DyeCycle (Life Technologies) then analyzed on Beckman Coulter Gallios 4. Male and female gametocytes were selected in the 820cl1 wild-type parasites and derived Pb*AT1-KO* parasites based on fluorescence, with male gametocytes selected by gating for GFP-positive cells and female gametocytes selected by gating for RFP-positive cells. The percentage of micro- and macro-gametocytes was expressed as a percentage of all parasite stages including asexual forms, whereas DNA replication status was expressed as a percentage of male gametocytes only. For each sample, >20,000 cells were analyzed.

Western blot analysis

Freshly egressed *T. gondii* parasites were pelleted and resuspended in RIPA buffer [150 mM NaCl, 1% Triton X-100, 0.5% deoxycholate, 0.1% SDS, 50 mM Tris-HCl pH 7.5 plus one tablet of a cOmplete protease inhibitor cocktail (Roche) per 200 µl] and incubated on ice for 15 min. This was followed by centrifugation at 18,400 ***g*** at 4°C for 15 min. The supernatant was separated from the pellet in a fresh tube and mixed with SDS–PAGE loading buffer under reducing conditions. The preparations were transferred onto nitrocellulose membranes and probed with appropriate antibodies in 5% non-fat milk powder dissolved in PBS containing 0.05% Tween-20. Proteins were detected through bound secondary peroxidase-conjugated antibodies using an ECL system (Amersham).

Intracellular growth

Confluent HFFs on coverslips were inoculated with *T. gondii* test strains and controls and left to grow for 24 h. The infected cells were fixed using PFA/GA and immunofluorescence assays followed using an anti-GAP45 antibody. The experiment was repeated three independent times, and 100 vacuoles were enumerated in each experiment. The data are presented as mean±s.d.

Lysis plaque assay

HFFs were seeded and grown to confluency before being inoculated with freshly egressed *T. gondii* parasites. The infected cells were allowed to sit for 7 d and were then fixed using PFA/GA. Plaque sizes were revealed by 0.1% Crystal Violet (Sigma) staining.

Parasite growth competition assay

In *P. berghei*, Pb*AT1-KO* parasites derived from the 820cl1 line and wild-type parasites of the 2.34 line were mixed in a 5:1 ratio and infected intraperitoneally into mice. Parasitemia was determined daily using flow cytometry, and Pb*AT1-KO* parasites were gated based on fluorescence. Mice were killed 6 d post infection based on total parasitemia.

In *T. gondii*, the Tg*AT1-KO* and RH (Tg) line were each mixed with GFP-expressing parasites expressing a copy of GFP under the control of the tubulin promoter (ptubGFP in an RH strain where Ku80 was deleted) at an estimated ratio of 80:20 (test strain:GFP strain). HFFs were inoculated with this mixture, and parasite ratios determined by flow cytometry at each passage as previously described (Nyonda et al., 2020).

MS-based quantitative proteomic analysis of the *T. gondii* lysine acetylome

Sample preparation

Five replicates of wild-type and Tg*AT1-KO* freshly egressed parasites were lysed from host cells by repeated passage through a syringe (3×, 28G) and subsequently purified by filtration (3 µm pore size; Millipore/Merck). The parasites were subsequently pelleted at 2800 ***g*** for 20 min at 4°C. Next, 1 ml of ice cold 8 M urea in 50 mM HEPES buffer with protease inhibitor [one tablet of cOmplete protease inhibitor cocktail (Roche)] at pH 6.6 was then added to the pellets, which were then resuspended gently using a pipette. This was followed by a sonication step of the samples at 4°C in an ultrasonic bath for 10 cycles (10 s sonication on and 30 s sonication off) and immediately transferred on ice. Extracted proteins were reduced using 20 mM dithiothreitol for 1 h at 37°C before alkylation with 55 mM iodoacetamide for 45 min at room temperature in the dark. The samples were then diluted using ammonium bicarbonate to obtain a urea concentration of 4 M. Proteins were digested with LysC (Promega) at a ratio of 1:200 for 4 h at 37°C. The samples were diluted again using ammonium bicarbonate to obtain a urea concentration of 1 M. Proteins were then digested with trypsin (Promega) at a ratio of 1:200 overnight at 37°C. Resulting peptides were purified by C18 reverse phase chromatography (Sep-Pak C18, Waters) before drying down.

Enrichment of acetylated peptides

Dried peptides were dissolved in IP buffer (100 mM NaCl, 1 mM EDTA, 20 mM Tris-HCl, 0.5% NP-40, pH 8). Acetylated peptides were mixed with anti-acetyl-lysine antibody immobilized on agarose beads (ImmuneChem, ICP0388) and incubated overnight at 4°C. Following incubation, the beads were washed twice with IP buffer, once with washing buffer (IP buffer without NP-40) and twice with ice cold ultra-pure water. Elution was performed using 0.1% trifluoroacetic acid. Enriched peptides were then dried down.

Nanoscale liquid chromatography–tandem mass spectrometry

The peptides were analyzed by online nanoscale liquid chromatography coupled to tandem MS (NanoLC–MS/MS; Ultimate 3000 RSLCnano coupled to a Q-Exactive HF; Thermo Fisher Scientific) using a 120-min gradient. Peptides were sampled on a 300 µm×5 mm PepMap C18 precolumn and separated on a 75 µm×250 mm C18 column (Reprosil-Pur 120 C18-AQ, 1.9 µm; Dr Maisch). MS and MS/MS data were acquired using the Xcalibur software (Thermo Fisher Scientific).

Identification and quantification of acetylated sites

MS RAW files were processed using MaxQuant (Tyanova et al., 2016). Spectra were searched against the *T. gondii* database (ME49 taxonomy, version 30 downloaded from ToxoDB), the Uniprot database (*Homo sapiens* taxonomy, 2020-11-27 version), the frequently observed contaminants database embedded in MaxQuant, and the corresponding reverse databases. Trypsin was chosen as the enzyme, and six missed cleavages were allowed. Precursor and fragment mass error tolerances were set at their default values. Peptide modifications allowed during the search were: carbamidomethyl (C, fixed), acetyl (protein N-term, variable), oxidation (M, variable) and acetyl (K, variable). Minimum number of peptides and razor+unique peptides were set to 1. Maximum false discovery rates were set to 0.01 at Peptide Spectrum Match (PSM), protein and site levels. The match between runs option was activated.

Statistical analyses

Statistical analyses were performed using ProStaR (Wieczorek et al., 2017). Only acetylated sites with a localization probability above 0.75 were considered. Peptides identified in the reverse and contaminant databases were discarded. For the comparison of acetylomes between the mutant strain and wild-type strains, acetylated sites were considered separately when they were identified on peptides bearing various numbers of acetylated sites to allow the quantification of the different peptidoforms. Only acetylated sites quantified in at least four replicates of one condition were conserved. After $\log_2$ transformation, acetylated site intensities were normalized using the vsn method before missing value imputation (slsa algorithm for partially observed values in the condition and DetQuantile algorithm for totally absent values in the condition). Statistical testing was conducted using limma. Differentially abundant acetylated sites were sorted out using the following cut-offs: $\log_2$(fold change) ≥ 1 or ≤ -1 and $P<0.01$, leading to a false discovery rate of <1% according to the Benjamini–Hochberg estimator. Acetylated sites found to be differentially abundant but identified by MS/MS in less than three replicates and detected in less than four replicates in the condition in which they were found to be more abundant were invalidated ($P=1$).

N-terminomics

The parasite pellets (Bienvenut et al., 2017b) were resuspended in 0.2 ml of lysis buffer consisting of 50 mM HEPES-NaOH, pH 7.2; 1.5 mM $MgCl_2$; 1 mM EGTA; 10% glycerol; 1% Triton X-100; 2 mM PMSF; EDTA+ protease inhibitor (Roche cOmplete protease inhibitor cocktail). The samples were briefly sonicated to ensure proper lysis, then incubated at 4°C for 1 h. Samples were centrifuged for 60 min at 4°C and 17,000 ***g***, the supernatants were collected and the protein amounts quantified using the Bradford method. 500 µg was then processed as described previously (Bienvenut et al., 2017a), with the exception of a few modifications detailed below. Briefly, the proteins extracted from the biological material were labeled on their N-termini and lysine ε-amino groups using N-acetoxy-[2H3] succinimide, before being subjected to trypsin digestion. The peptides obtained were then fractionated using strong cation exchange chromatography, and fractions 2–11 were individually analyzed on an LTQ-Orbitrap velos mass spectrometer (Thermo Fisher Scientific) coupled to a liquid chromatography. The data obtained were processed using Mascot Distiller, searching against a custom ME49-based *T. gondii* protein database (v.30) or a *P. berghei* reference proteome set (UP000074855), as appropriate, with the parent and fragment mass tolerance defined as 10 ppm and 0.5 Da, respectively. The quantitation results, along with each Mascot search output, were then parsed using the EnCOUNTer script (Bienvenut et al., 2017b) to obtain the final N-terminal acetylome datasets.

The analyzed samples corresponded to the RHΔKU80 *T. gondii* strain (wild-type), and the *AT1*-KO mutant (Tg*AT1*-KO), and to the ANKA *P. berghei* strain and the corresponding *AT1*-KO mutant (Pb*AT1*-KO), with either three or two distinct biological replicates of each condition performed for *T. gondii* and *P. berghei* samples, respectively.

Acknowledgements

We thank Jean-Baptiste Marq and Aurelia Balestra for technical assistance. We also thank the Bioimaging and Flow Cytometry core facilities at the Faculty of Medicine, University of Geneva.

Competing interests

The authors declare no competing or financial interests.

Author contributions

Conceptualization: T.M., D.S.-F., C.G.; Methodology: M.A.N., L.B., P.P., Y.C., M.B., T.M., D.S.-F., C.G.; Validation: T.M., D.S.-F., C.G.; Formal analysis: M.A.N., J.-B.B., L.B., P.P., Y.C., M.B., T.M., D.S.-F., C.G.; Investigation: M.A.N., J.-B.B., L.B., A.K., P.P., Y.C., M.B., T.M., D.S.-F., C.G.; Writing - original draft: M.A.N., T.M., C.G.; Writing - review & editing: M.A.N., L.B., A.K., P.P., Y.C., M.B., T.M., D.S.-F., C.G.; Visualization: A.K., T.M., C.G.; Supervision: T.M., D.S.-F., C.G.; Project administration: M.A.N., T.M., D.S.-F., C.G.; Funding acquisition: T.M., D.S.-F., C.G.

Funding

This research was supported by the European Research Council (ERC) under the European Union's Horizon 2020 research and innovation program agreement 695596 to D.S.-F.; by 51RTP0_151032 (MalarX), a SystemsX grant awarded by the Schweizerischer Nationalfonds zur Förderung der Wissenschaftlichen Forschung to D.S.-F.; by KatNat (ERA-NET, ANR-17-CAPS-0001-01) and CanMore (France–Germany PRCI, ANR-20 CE92-0040) grants funded by Agence Nationale de la Recherche to C.G. for support of J.B.B.; by Fondation ARC pour la Recherche sur le Cancer (ARCPJA32020060002137) grants to T.M.; and from the facilities and expertise of the I2BC proteomic platform SICaPS, supported by Infrastructures en Biologie Santé et Agronomie (IBiSA), Agence Régionale de Santé Île-de-France, Plan Cancer, Centre National de la Recherche Scientifique and Université Paris-Sud. The proteomic experiments were partly supported by Agence Nationale de la Recherche under projects ProFI (Proteomics French Infrastructure, ANR-10-INBS-08) and GRAL, a program from the Chemistry Biology Health (CBH) Graduate School of Université Grenoble Alpes (ANR-17-EURE-0003).

Data availability

Mass spectrometry proteomics data associated with the N-terminal and lysine acetylomes have been deposited at ProteomeXchange via the PRIDE repository (Vizcaíno et al., 2013) with the dataset identifiers: PXD029616 and PXD030932.

Peer review history

The peer review history is available online at https://journals.biologists.com/jcs/article-lookup/doi/10.1242/jcs.259811.

References

Aksnes, H., Drazic, A., Marie, M. and Arnesen, T. (2016). First things first: vital protein marks by N-terminal acetyltransferases. *Trends Biochem. Sci.* **41**, 746-760. doi:10.1016/j.tibs.2016.07.005

Aksnes, H., Ree, R. and Arnesen, T. (2019). Co-translational, post-translational, and non-catalytic roles of N-terminal acetyltransferases. *Mol. Cell* **73**, 1097-1114. doi:10.1016/j.molcel.2019.02.007

Balestra, A. C., Koussis, K., Klages, N., Howell, S. A., Flynn, H. R., Bantscheff, M., Pasquarello, C., Perrin, A. J., Brusini, L., Arboit, P. et al. (2021). Ca2+ signals critical for egress and gametogenesis in malaria parasites depend on a multipass membrane protein that interacts with PKG. *Sci. Adv.* **7**, eabe5396. doi:10.1126/sciadv.abe5396

Balestra, A. C., Zeeshan, M., Rea, E., Pasquarello, C., Brusini, L., Mourier, T., Subudhi, A. K., Klages, N., Arboit, P., Pandey, R. et al. (2020). A divergent cyclin/cyclin-dependent kinase complex controls the atypical replication of a malaria parasite during gametogony and transmission. *eLife* **9**, e56474. doi:10.7554/eLife.56474

Barylyuk, K., Koreny, L., Ke, H., Butterworth, S., Crook, O. M., Lassadi, I., Gupta, V., Tromer, E., Mourier, T., Stevens, T. J. et al. (2020). A comprehensive subcellular atlas of the *toxoplasma* proteome via hyperLOPIT provides spatial context for protein functions. *Cell Host Microbe* **28**, 752-766.e9. doi:10.1016/j.chom.2020.09.011

Bienvenut, W. V., Giglione, C. and Meinnel, T. (2015). Proteome-wide analysis of the amino terminal status of Escherichia coli proteins at the steady-state and upon deformylation inhibition. *Proteomics* **15**, 2503-2518. doi:10.1002/pmic.201500027

Bienvenut, W. V., Giglione, C. and Meinnel, T. (2017a). SILProNAQ: a convenient approach for proteome-wide analysis of protein N-termini and N-terminal acetylation quantitation. *Methods Mol. Biol.* **1574**, 17-34. doi:10.1007/978-1-4939-6850-3_3

Bienvenut, W. V., Scarpelli, J. P., Dumestier, J., Meinnel, T. and Giglione, C. (2017b). EnCOUNTer: a parsing tool to uncover the mature N-terminus of organelle-targeted proteins in complex samples. *BMC Bioinformatics* **18**, 182. doi:10.1186/s12859-017-1595-y

Bienvenut, W. V., Brunje, A., Boyer, J. B., Muhlenbeck, J. S., Bernal, G., Lassowskat, I., Dian, C., Linster, E., Dinh, T. V., Koskela, M. M. et al. (2020). Dual lysine and N-terminal acetyltransferases reveal the complexity underpinning protein acetylation. *Mol. Syst. Biol.* **16**, e9464. doi:10.15252/msb.20209464

Billker, O., Lindo, V., Panico, M., Etienne, A. E., Paxton, T., Dell, A., Rogers, M., Sinden, R. E. and Morris, H. R. (1998). Identification of xanthurenic acid as the putative inducer of malaria development in the mosquito. *Nature* **392**, 289-292. doi:10.1038/32667

Billker, O., Dechamps, S., Tewari, R., Wenig, G., Franke-Fayard, B. and Brinkmann, V. (2004). Calcium and a calcium-dependent protein kinase regulate gamete formation and mosquito transmission in a malaria parasite. *Cell* **117**, 503-514. doi:10.1016/S0092-8674(04)00449-0

Boddey, J. A., Hodder, A. N., Günther, S., Gilson, P. R., Patsiouras, H., Kapp, E. A., Pearce, J. A., De Koning-Ward, T. F., Simpson, R. J., Crabb, B. S. et al. (2010). An aspartyl protease directs malaria effector proteins to the host cell. *Nature* **463**, 627-631. doi:10.1038/nature08728

Brown, K. M., Long, S. and Sibley, L. D. (2018). Conditional knockdown of proteins using Auxin-inducible Degron (AID) fusions in *Toxoplasma gondii*. *Bio. Protoc.* **8**, e2728. doi:10.21769/BioProtoc.2728

Bushell, E., Gomes, A. R., Sanderson, T., Anar, B., Girling, G., Herd, C., Metcalf, T., Modrzynska, K., Schwach, F., Martin, R. E. et al. (2017). Functional profiling of a *Plasmodium* genome reveals an abundance of essential genes. *Cell* **170**, 260-272.e8. doi:10.1016/j.cell.2017.06.030

Chanda, I., Pan, A. and Dutta, C. (2005). Proteome composition in *Plasmodium falciparum*: higher usage of GC-rich nonsynonymous codons in highly expressed genes. *J. Mol. Evol.* **61**, 513-523. doi:10.1007/s00239-005-0023-5

Chang, H. H., Falick, A. M., Carlton, P. M., Sedat, J. W., Derisi, J. L. and Marletta, M. A. (2008). N-terminal processing of proteins exported by malaria parasites. *Mol. Biochem. Parasitol.* **160**, 107-115. doi:10.1016/j.molbiopara.2008.04.011

Cobbold, S. A., Vaughan, A. M., Lewis, I. A., Painter, H. J., Camargo, N., Perlman, D. H., Fishbaugher, M., Healer, J., Cowman, A. F., Kappe, S. H. I. et al. (2013). Kinetic flux profiling elucidates two independent acetyl-CoA biosynthetic pathways in *Plasmodium falciparum*. *J. Biol. Chem.* **288**, 36338-36350. doi:10.1074/jbc.M113.503557

Cobbold, S. A., Santos, J. M., Ochoa, A., Perlman, D. H. and Llinas, M. (2016). Proteome-wide analysis reveals widespread lysine acetylation of major protein complexes in the malaria parasite. *Sci. Rep.* **6**, 19722. doi:10.1038/srep19722

Coffey, M. J., Sleebs, B. E., Uboldi, A. D., Garnham, A., Franco, M., Marino, N. D., Panas, M. W., Ferguson, D. J., Enciso, M., O'Neill, M. T. et al. (2015). An aspartyl protease defines a novel pathway for export of *Toxoplasma* proteins into the host cell. *eLife* **4**, e10809. doi:10.7554/eLife.10809

Coffey, M. J., Dagley, L. F., Seizova, S., Kapp, E. A., Infusini, G., Roos, D. S., Boddey, J. A., Webb, A. I. and Tonkin, C. J. (2018). Aspartyl protease 5 matures dense granule proteins that reside at the host-parasite interface in *Toxoplasma gondii*. *mBio* **9**, e01796-18. doi:10.1128/mBio.01796-18

Cova, M., López-Gutiérrez, B., Artigas-Jerónimo, S., González-Díaz, A., Bandini, G., Maere, S., Carretero-Paulet, L. and Izquierdo, L. (2018). The Apicomplexa-specific glucosamine-6-phosphate N-acetyltransferase gene family encodes a key enzyme for glycoconjugate synthesis with potential as therapeutic target. *Sci. Rep.* **8**, 4005. doi:10.1038/s41598-018-22441-3

De Vries, L. E., Lunghi, M., Krishnan, A., Kooij, T. W. A. and Soldati-Favre, D. (2021). Pantothenate and CoA biosynthesis in Apicomplexa and their promise as antiparasitic drug targets. *PLoS Pathog.* **17**, e1010124. doi:10.1371/journal.ppat.1010124

Dieterich, I. A., Lawton, A. J., Peng, Y., Yu, Q., Rhoads, T. W., Overmyer, K. A., Cui, Y., Armstrong, E. A., Howell, P. R., Burhans, M. S. et al. (2019). Acetyl-CoA flux regulates the proteome and acetyl-proteome to maintain intracellular metabolic crosstalk. *Nat. Commun.* **10**, 3929. doi:10.1038/s41467-019-11945-9

Ding, M., Clayton, C. and Soldati, D. (2000). Toxoplasma gondii catalase: are there peroxisomes in toxoplasma? *J. Cell Sci.* **113**, 2409-2419. doi:10.1242/jcs.113.13.2409

Doerig, C., Rayner, J. C., Scherf, A. and Tobin, A. B. (2015). Post-translational protein modifications in malaria parasites. *Nat. Rev. Microbiol.* **13**, 160-172. doi:10.1038/nrmicro3402

Dogga, S. K., Mukherjee, B., Jacot, D., Kockmann, T., Molino, L., Hammoudi, P.-M., Hartkoorn, R. C., Hehl, A. B. and Soldati-Favre, D. (2017). A druggable secretory protein maturase of *Toxoplasma* essential for invasion and egress. *eLife* **6**, e27480. doi:10.7554/eLife.27480

Donald, R. G. and Roos, D. S. (1993). Stable molecular transformation of *Toxoplasma gondii:* a selectable dihydrofolate reductase-thymidylate synthase marker based on drug-resistance mutations in malaria. *Proc. Natl. Acad. Sci. USA* **90**, 11703-11707. doi:10.1073/pnas.90.24.11703

Donald, R. G. K., Carter, D., Ullman, B. and Roos, D. S. (1996). Insertional tagging, cloning, and expression of the *Toxoplasma gondii* hypoxanthine-xanthine-guanine phosphoribosyltransferase gene. Use as a selectable marker for stable transformation. *J. Biol. Chem.* **271**, 14010-14019. doi:10.1074/jbc.271.24.14010

Drazic, A., Myklebust, L. M., Ree, R. and Arnesen, T. (2016). The world of protein acetylation. *Biochim. Biophys. Acta* **1864**, 1372-1401. doi:10.1016/j.bbapap.2016.06.007

Fang, H., Klages, N., Baechler, B., Hillner, E., Yu, L., Pardo, M., Choudhary, J. and Brochet, M. (2017). Multiple short windows of calcium-dependent protein kinase 4 activity coordinate distinct cell cycle events during *Plasmodium* gametogenesis. *eLife* **6**, e26524. doi:10.7554/eLife.26524

Farrugia, M. A. and Puglielli, L. (2018). Nepsilon-lysine acetylation in the endoplasmic reticulum - a novel cellular mechanism that regulates proteostasis and autophagy. *J. Cell Sci.* **131**, jcs221747. doi:10.1242/jcs.221747

Fleige, T., Fischer, K., Ferguson, D. J. P., Gross, U. and Bohne, W. (2007). Carbohydrate metabolism in the Toxoplasma gondii apicoplast: localization of three glycolytic isoenzymes, the single pyruvate dehydrogenase complex, and a plastid phosphate translocator. *Eukaryot. Cell* **6**, 984-996. doi:10.1128/EC.00061-07

Forte, G. M. A., Pool, M. R. and Stirling, C. J. (2011). N-terminal acetylation inhibits protein targeting to the endoplasmic reticulum. *PLoS Biol.* **9**, e1001073. doi:10.1371/journal.pbio.1001073

Fox, B. A., Ristuccia, J. G., Gigley, J. P. and Bzik, D. J. (2009). Efficient gene replacements in *Toxoplasma gondii* strains deficient for nonhomologous end joining. *Eukaryot. Cell* **8**, 520-529. doi:10.1128/EC.00357-08

Frenal, K., Marq, J.-B., Jacot, D., Polonais, V. and Soldati-Favre, D. (2014). Plasticity between MyoC- and MyoA-glideosomes: an example of functional compensation in *Toxoplasma gondii* invasion. *PLoS Pathog.* **10**, e1004504. doi:10.1371/journal.ppat.1004504

Friedmann, D. R. and Marmorstein, R. (2013). Structure and mechanism of non-histone protein acetyltransferase enzymes. *FEBS J.* **280**, 5570-5581. doi:10.1111/febs.12373

Frottin, F., Espagne, C., Traverso, J. A., Mauve, C., Valot, B., Lelarge-Trouverie, C., Zivy, M., Noctor, G., Meinnel, T. and Giglione, C. (2009). Cotranslational proteolysis dominates glutathione homeostasis to support proper growth and development. *Plant Cell* **21**, 3296-3314. doi:10.1105/tpc.109.069757

Frottin, F., Bienvenut, W. V., Bignon, J., Jacquet, E., Vaca Jacome, A. S., Van Dorsselaer, A., Cianferani, S., Carapito, C., Meinnel, T. and Giglione, C. (2016). MetAP1 and MetAP2 drive cell selectivity for a potent anti-cancer agent in synergy, by controlling glutathione redox state. *Oncotarget* **7**, 63306-63323. doi:10.18632/oncotarget.11216

Gardner, M. J., Hall, N., Fung, E., White, O., Berriman, M., Hyman, R. W., Carlton, J. M., Pain, A., Nelson, K. E., Bowman, S. et al. (2002). Genome sequence of the human malaria parasite *Plasmodium falciparum*. *Nature* **419**, 498-511. doi:10.1038/nature01097

Giglione, C. and Meinnel, T. (2021). Evolution-driven versatility of N terminal acetylation in photoautotrophs. *Trends Plant Sci.* **26**, 375-391. doi:10.1016/j.tplants.2020.11.012

Giglione, C., Fieulaine, S. and Meinnel, T. (2015). N-terminal protein modifications: Bringing back into play the ribosome. *Biochimie* **114**, 134-146. doi:10.1016/j.biochi.2014.11.008

Goyal, M., Alam, A., Iqbal, M. S., Dey, S., Bindu, S., Pal, C., Banerjee, A., Chakrabarti, S. and Bandyopadhyay, U. (2012). Identification and molecular characterization of an Alba-family protein from human malaria parasite *Plasmodium falciparum*. *Nucleic Acids Res.* **40**, 1174-1190. doi:10.1093/nar/gkr821

Hammoudi, P.-M., Jacot, D., Mueller, C., Di Cristina, M., Dogga, S. K., Marq, J.-B., Romano, J., Tosetti, N., Dubrot, J., Emre, Y. et al. (2015). Fundamental roles of the Golgi-associated *Toxoplasma* aspartyl protease, ASP5, at the host-parasite interface. *PLoS Pathog.* **11**, e1005211. doi:10.1371/journal.ppat.1005211

Hirabayashi, Y., Kanamori, A., Nomura, K. H. and Nomura, K. (2004). The acetyl-CoA transporter family SLC33. *Pflugers Arch.* **447**, 760-762. doi:10.1007/s00424-003-1071-6

Hirabayashi, Y., Nomura, K. H. and Nomura, K. (2013). The acetyl-CoA transporter family SLC33. *Mol. Aspects Med.* **34**, 586-589. doi:10.1016/j.mam.2012.05.009

Jeffers, V. and Sullivan, W. J.Jr. (2012). Lysine acetylation is widespread on proteins of diverse function and localization in the protozoan parasite *Toxoplasma gondii*. *Eukaryot. Cell* **11**, 735-742. doi:10.1128/EC.00088-12

Jonas, M. C., Pehar, M. and Puglielli, L. (2010). AT-1 is the ER membrane acetyl-CoA transporter and is essential for cell viability. *J. Cell Sci.* **123**, 3378-3388. doi:10.1242/jcs.068841

Kloehn, J., Oppenheim, R. D., Siddiqui, G., De Bock, P.-J., Kumar Dogga, S., Coute, Y., Hakimi, M.-A., Creek, D. J. and Soldati-Favre, D. (2020). Multi-omics analysis delineates the distinct functions of sub-cellular acetyl-CoA pools in *Toxoplasma gondii*. *BMC Biol.* **18**, 67. doi:10.1186/s12915-020-00791-7

Ko, M. H. and Puglielli, L. (2009). Two endoplasmic reticulum (ER)/ER Golgi intermediate compartment-based lysine acetyltransferases post-translationally

regulate BACE1 levels. *J. Biol. Chem.* **284**, 2482-2492. doi:10.1074/jbc.M804901200

Krishnan, A., Kloehn, J., Lunghi, M., Chiappino-Pepe, A., Waldman, B. S., Nicolas, D., Varesio, E., Hehl, A., Lourido, S., Hatzimanikatis, V. et al. (2020). Functional and computational genomics reveal unprecedented flexibility in stage-specific *Toxoplasma* metabolism. *Cell Host Microbe* **27**, 290-306.e11. doi:10.1016/j.chom.2020.01.002

Lim, M. Y.-X., LaMonte, G., Lee, M. C. S., Reimer, C., Tan, B. H., Corey, V., Tjahjadi, B. F., Chua, A., Nachon, M., Wintjens, R. et al. (2016). UDP-galactose and acetyl-CoA transporters as *Plasmodium* multidrug resistance genes. *Nat. Microbiol.* **1**, 16166. doi:10.1038/nmicrobiol.2016.166

Linster, E. and Wirtz, M. (2018). N-terminal acetylation: an essential protein modification emerges as an important regulator of stress responses. *J. Exp. Bot.* **69**, 4555-4568. doi:10.1093/jxb/ery241

Mair, G. R., Lasonder, E., Garver, L. S., Franke-Fayard, B. M. D., Carret, C. K., Wiegant, J. C. A. G., Dirks, R. W., Dimopoulos, G., Janse, C. J. and Waters, A. P. (2010). Universal features of post-transcriptional gene regulation are critical for *Plasmodium* zygote development. *PLoS Pathog.* **6**, e1000767. doi:10.1371/journal.ppat.1000767

Mak, A. B., Pehar, M., Nixon, A. M. L., Williams, R. A., Uetrecht, A. C., Puglielli, L. and Moffat, J. (2014). Post-translational regulation of CD133 by ATase1/ATase2-mediated lysine acetylation. *J. Mol. Biol.* **426**, 2175-2182. doi:10.1016/j.jmb.2014.02.012

Mallo, N., Ovciarikova, J., Martins-Duarte, E. S., Baehr, S. C., Biddau, M., Wilde, M.-L., Uboldi, A. D., Lemgruber, L., Tonkin, C. J., Wideman, J. G. et al. (2021). Depletion of a *Toxoplasma* porin leads to defects in mitochondrial morphology and contacts with the endoplasmic reticulum. *J. Cell Sci.* **134**, jcs255299. doi:10.1242/jcs.255299

Martinez, A., Traverso, J. A., Valot, B., Ferro, M., Espagne, C., Ephritikhine, G., Zivy, M., Giglione, C. and Meinnel, T. (2008). Extent of N-terminal modifications in cytosolic proteins from eukaryotes. *Proteomics* **8**, 2809-2831. doi:10.1002/pmic.200701191

Meinnel, T., Dian, C. and Giglione, C. (2020). Myristoylation, an ancient protein modification mirroring eukaryogenesis and evolution. *Trends Biochem. Sci.* **45**, 619-632. doi:10.1016/j.tibs.2020.03.007

Moll, K., Kaneko, A., Scherf, A. and Wahlgren, M. (2013). *Methods in malaria research*. 6th Edition. EVIMalaR.

Montgomery, D. C., Sorum, A. W. and Meier, J. L. (2015). Defining the orphan functions of lysine acetyltransferases. *ACS Chem. Biol.* **10**, 85-94. doi:10.1021/cb500853p

Muñoz, E. E., Hart, K. J., Walker, M. P., Kennedy, M. F., Shipley, M. M. and Lindner, S. E. (2017). ALBA4 modulates its stage-specific interactions and specific mRNA fates during *Plasmodium yoelii* growth and transmission. *Mol. Microbiol.* **106**, 266-284. doi:10.1111/mmi.13762

Nyonda, M. A., Hammoudi, P. M., Ye, S., Maire, J., Marq, J. B., Yamamoto, M. and Soldati-Favre, D. (2020). *Toxoplasma gondii* GRA60 is an effector protein that modulates host cell autonomous immunity and contributes to virulence. *Cell. Microbiol.*, **23**, e13278.

Osborne, A. R., Speicher, K. D., Tamez, P. A., Bhattacharjee, S., Speicher, D. W. and Haldar, K. (2010). The host targeting motif in exported *Plasmodium* proteins is cleaved in the parasite endoplasmic reticulum. *Mol. Biochem. Parasitol.* **171**, 25-31. doi:10.1016/j.molbiopara.2010.01.003

Pehar, M. and Puglielli, L. (2013). Lysine acetylation in the lumen of the ER: a novel and essential function under the control of the UPR. *Biochim. Biophys. Acta* **1833**, 686-697. doi:10.1016/j.bbamcr.2012.12.004

Pieperhoff, M. S., Pall, G. S., Jiménez-Ruiz, E., Das, S., Melatti, C., Gow, M., Wong, E. H., Heng, J., Müller, S., Blackman, M. J. et al. (2015). Conditional U1 Gene Silencing in *Toxoplasma gondii*. *PLoS One* **10**, e0130356. doi:10.1371/journal.pone.0130356

Pietrocola, F., Galluzzi, L., Bravo-San Pedro, J. M., Madeo, F. and Kroemer, G. (2015). Acetyl coenzyme A: a central metabolite and second messenger. *Cell Metab.* **21**, 805-821. doi:10.1016/j.cmet.2015.05.014

Plattner, F., Yarovinsky, F., Romero, S., Didry, D., Carlier, M.-F., Sher, A. and Soldati-Favre, D. (2008). *Toxoplasma* profilin is essential for host cell invasion and TLR11-dependent induction of an interleukin-12 response. *Cell Host Microbe* **3**, 77-87. doi:10.1016/j.chom.2008.01.001

Rathore, O. S., Faustino, A., Prudêncio, P., Van Damme, P., Cox, C. J. and Martinho, R. G. (2016). Absence of N-terminal acetyltransferase diversification during evolution of eukaryotic organisms. *Sci. Rep.* **6**, 21304. doi:10.1038/srep21304

Reddy, B. P. N., Shrestha, S., Hart, K. J., Liang, X., Kemirembe, K., Cui, L. and Lindner, S. E. (2015). A bioinformatic survey of RNA-binding proteins in *Plasmodium*. *BMC Genomics* **16**, 890. doi:10.1186/s12864-015-2092-1

Russo, I., Babbitt, S., Muralidharan, V., Butler, T., Oksman, A. and Goldberg, D. E. (2010). Plasmepsin V licenses *Plasmodium* proteins for export into the host erythrocyte. *Nature* **463**, 632-636. doi:10.1038/nature08726

Sheiner, L. and Soldati-Favre, D. (2008). Protein trafficking inside Toxoplasma gondii. *Traffic* **9**, 636-646. doi:10.1111/j.1600-0854.2008.00713.x

Shen, B., Brown, K. M., Lee, T. D. and Sibley, L. D. (2014). Efficient gene disruption in diverse strains of *Toxoplasma gondii* using CRISPR/CAS9. *mBio* **5**, e01114-14. doi:10.1128/mBio.01114-14

Sidik, S. M., Huet, D., Ganesan, S. M., Huynh, M.-H., Wang, T., Nasamu, A. S., Thiru, P., Saeij, J. P. J., Carruthers, V. B., Niles, J. C. et al. (2016). A genome-wide CRISPR screen in *Toxoplasma* identifies essential apicomplexan genes. *Cell* **166**, 1423-1435.e12. doi:10.1016/j.cell.2016.08.019

Soldati, D. and Boothroyd, J. C. (1993). Transient transfection and expression in the obligate intracellular parasite *Toxoplasma gondii*. *Science* **260**, 349-352. doi:10.1126/science.8469986

Stanway, R. R., Bushell, E., Chiappino-Pepe, A., Roques, M., Sanderson, T., Franke-Fayard, B., Caldelari, R., Golomingi, M., Nyonda, M., Pandey, V. et al. (2019). Genome-scale identification of essential metabolic processes for targeting the *Plasmodium* liver stage. *Cell* **179**, 1112-1128.e26. doi:10.1016/j.cell.2019.10.030

Tyanova, S., Temu, T. and Cox, J. (2016). The MaxQuant computational platform for mass spectrometry-based shotgun proteomics. *Nat. Protoc.* **11**, 2301-2319. doi:10.1038/nprot.2016.136

Tymoshenko, S., Oppenheim, R. D., Agren, R., Nielsen, J., Soldati-Favre, D. and Hatzimanikatis, V. (2015). Metabolic needs and capabilities of *Toxoplasma gondii* through combined computational and experimental analysis. *PLoS Comput. Biol.* **11**, e1004261. doi:10.1371/journal.pcbi.1004261

Van Damme, P., Lasa, M., Polevoda, B., Gazquez, C., Elosegui-Artola, A., Kim, D. S., De Juan-Pardo, E., Demeyer, K., Hole, K., Larrea, E. et al. (2012). N-terminal acetylome analyses and functional insights of the N-terminal acetyltransferase NatB. *Proc. Natl. Acad. Sci. USA* **109**, 12449-12454. doi:10.1073/pnas.1210303109

Varland, S., Aksnes, H., Kryuchkov, F., Impens, F., Van Haver, D., Jonckheere, V., Ziegler, M., Gevaert, K., Van Damme, P. and Arnesen, T. (2018). N-terminal acetylation levels are maintained during acetyl-CoA deficiency in *Saccharomyces cerevisiae*. *Mol. Cell. Proteomics* **17**, 2309-2323. doi:10.1074/mcp.RA118.000982

Vembar, S. S., Macpherson, C. R., Sismeiro, O., Coppee, J.-Y. and Scherf, A. (2015). The PfAlba1 RNA-binding protein is an important regulator of translational timing in *Plasmodium falciparum* blood stages. *Genome Biol.* **16**, 212. doi:10.1186/s13059-015-0771-5

Vincke, I. H. and Lips, M. (1948). A new plasmodium from a wild Congo rodent *Plasmodium berghei* n. *sp. Ann. Soc. Belg. Med. Trop. (1920)* **28**, 97-104.

Vizcaíno, J. A., Côté, R. G., Csordas, A., Dianes, J. A., Fabregat, A., Foster, J. M., Griss, J., Alpi, E., Birim, M., Contell, J. et al. (2013). The PRoteomics IDEntifications (PRIDE) database and associated tools: status in 2013. *Nucleic Acids Res.* **41**, D1063-D1069. doi:10.1093/nar/gks1262

Volkmann, K., Pfander, C., Burstroem, C., Ahras, M., Goulding, D., Rayner, J. C., Frischknecht, F., Billker, O. and Brochet, M. (2012). The alveolin IMC1h is required for normal ookinete and sporozoite motility behaviour and host colonisation in Plasmodium berghei. *PLoS ONE* **7**, e41409. doi:10.1371/journal.pone.0041409

Wieczorek, S., Combes, F., Lazar, C., Giai Gianetto, Q., Gatto, L., Dorffer, A., Hesse, A.-M., Couté, Y., Ferro, M., Bruley, C. et al. (2017). DAPAR & ProStaR: software to perform statistical analyses in quantitative discovery proteomics. *Bioinformatics* **33**, 135-136. doi:10.1093/bioinformatics/btw580

Xue, B., Jeffers, V., Sullivan, W. J. and Uversky, V. N. (2013). Protein intrinsic disorder in the acetylome of intracellular and extracellular *Toxoplasma gondii*. *Mol. Biosyst.* **9**, 645-657. doi:10.1039/c3mb25517d

Zhang, M., Wang, C., Otto, T. D., Oberstaller, J., Liao, X., Adapa, S. R., Udenze, K., Bronner, I. F., Casandra, D., Mayho, M. et al. (2018). Uncovering the essential genes of the human malaria parasite *Plasmodium falciparum* by saturation mutagenesis. *Science* **360**, eaap7847. doi:10.1126/science.aap7847